DETERMINATION OF MARINE SEDIMENT STRENGTH AT DEPTH FROM IODP DRILLING DATA, NANTROSEIZE TRANSECT

A Thesis

by

DANA LU GALLEGOS

Submitted to the Office of Graduate and Professional Studies of
Texas A&M University
in partial fulfillment of the requirements for the degree of

MASTER OF SCIENCE

Chair of Committee,	Frederick M. Chester
Committee Members,	Hiroko Kitajima
	Charles P. Aubeny
Head of Department,	Michael C. Pope

May 2019

Major Subject: Geophysics

ABSTRACT

Earthquakes and tsunami events pose significant threats to human life and property. Accordingly, the scientific community is developing an understanding of what controls fault strength and failure mechanics in order to develop physics-based models for predicting earthquake-related phenomena. Subduction zones, such as the Nankai Trough offshore South Japan, are particularly susceptible to damaging earthquakes and tsunamis, e.g., the events of 1944 Tonankai (M8.1) and 1946 Nankaido (M8.3) earthquakes. A series of scientific boreholes was drilled through marine sediments across the Nankai Trough Seismogenic Zone by the International Ocean Discovery Program (NanTroSEIZE transect, IODP) to acquire geologic and geophysical data that may be used to characterize the geomechanical properties relevant to fault strength and failure mechanics. To better define the mechanical behavior of marine sediments in subduction zones, NanTroSEIZE drilling data are analyzed and modeled to characterize sediment mechanical response and strength as a function of depth, lithology and tectonic loading history. New methods are developed herein based on previous work in the mining and petroleum industry that relate drilling performance parameters to rock strength, and on geotechnical and geophysical understanding of marine sediment properties. The methodology is applied to drilling data from two sites of the NanTroSEIZE transect, IODP Sites C0006 and C0011, to evaluate the differences between the tectonically deformed sediments within the frontal portion of the accretionary prism and the less deformed sediments at the outer rise of the incoming

plate. Using the data analysis and modeling methods, and employing a novel Relative Drillability relationship, both the overall change in strength of sediment with depth due to burial consolidation, and the second-order deviations in strength due to lithology, in situ stress, and sediment burial history, can be characterized from drilling data for both IODP Sites. The findings are consistent with the hypothesis that the incoming sediments are relatively weaker than those accreted at the frontal thrust of the accretionary prism, and demonstrate the potential for utilizing the drilling data commonly acquired during IODP operations to quantify profiles of sediment strength versus depth.

CONTRIBUTORS AND FUNDING SOURCES

This work was supported by a thesis committee consisting of Dr. Frederick Chester (advisor) and Dr. Hiroko Kitajima of the Department of Geology and Geophysics and Dr. Charles Aubeny of the Department of Civil Engineering.

The drilling data analyzed for the entirety of the project was provided by Dr. Frederick Chester and Dr. Hiroko Kitajima from on-ship operations. The relationships presented in Chapters V through VII were also initially proposed by Dr. Frederick Chester and Dr. Hiroko Kitajima. All lithologic, operations, and geomechanical information was provided by the IODP Expedition scientists from the public data website http://sio7.jamstec.go.jp/. All other work conducted for the thesis was completed by the student independently.

Graduate study was supported by a fellowship from Texas A&M University, Teaching Assistantship stipends, and funding support from Dr. Frederick Chester.

NOMENCLATURE

A	Area of Bit [m^2]
BHA	Bottom Hole Assembly
d_I	Inner Bit Diameter [m]
d_O	Outer Bit Diameter [m]
η	Bit Efficiency Factor
d	Effective Bit Diameter [m]
ESCS	Extended Shoe Coring System
DBML	Depth Below Mud Line [m]
HPS	Hydraulic Powered Swivel
LWD	Logging While Drilling
MBSF	Meters Below Seafloor [m]
MBSL	Meters Below Sea-level [m]
$E'_{s\,min}$	Minimum Specific Energy [kPa]
σ	Normal Stress [kPa]
PDC	Polycrystalline Diamond Compact Bit
$Relative\ Drillability_{F,T}$	Relative Drillability for Force (F) and Torque (T)
u	Rate of Penetration (ROP) [m/min]
RCB	Rotary Core Barrel
$E'_{s\,T}$	Rotational Component Specific Energy [kPa]
N	Rotary Speed [revolutions per minute (rpm)]

τ	Shear Strength [kPa]
a_F	Slope of Force Performance Curve [m^2/kN]
a_T	Slope of Torque Performance Curve [m^2/kN]
E'_s	Specific Energy of the Rock [kPa]
T_c	Threshold Torque [kN/m]
F_c	Threshold Weight [kN/m]
$E'_{s\,F}$	Thrust Component Specific Energy [kPa]
T	Torque [kN-m]
TD	Total Depth [m]

TABLE OF CONTENTS

Page

LIST OF FIGURES

Page

LIST OF TABLES

Page

CHAPTER I

INTRODUCTION

Earthquakes have long been studied due to devastating human and financial losses occurred during large slip events. Subduction zones in particular have a long history of producing most of the largest earthquake events, and as such there is desire to understand fault strength and failure mechanics to improve physics-based hazard assessment and probabilistic forecasting. Physics-based models depend on underlying assumptions regarding the geomechanical behavior of sediments including factors such as in situ stress state, fluid pressure, sediment composition, and consolidation state (Tobin & Kinoshita, 2007; Kitajima et al., 2012). One such geomechanical model is the elastic-plastic, Coulomb wedge model of accretionary prisms by Wang and Hu (2006), which illustrates the relationship between the stress state within accretionary prisms over the earthquake cycle and the activation of faults leading to tsunami generation. In situ stress state is difficult to measure directly and thus is commonly inferred from sediment mechanical properties, which also are challenging to measure directly. For example, the elastic-plastic wedge model can estimate the stress state within the wedge by assuming sediment cohesion and coefficient of internal friction values, but these and other parameters (e.g., fluid pressure) are poorly known and thus solutions for stress are very uncertain (Wang and Hu, 2006).

The Nankai subduction zone constitutes a major earthquake and tsunami hazard to southern Japan, and recently has been the focus of an Integrated Ocean Discovery

Program (IODP) complex drilling project to collect geological and geophysical information, including sediment strength, along a transect across the zone. The most robust method currently available to determine sediment strength is through experimental deformation of core samples in the laboratory; however, experimental work is often time and labor intensive and in practice is often limited to just a few samples from discrete depth intervals (Saffer et al., 2011; Song et al., 2011; Kitajima et al., 2012). Experimental measurements also require core samples which are expensive and difficult to obtain and properly preserve. Knowledge of sediment strength is used to quantify in-situ stress state from observation of well-bore failures in image logs; specifically, material properties including uniaxial compressive strength (UCS) and angle of internal friction must be known (Chang et al., 2010; Song et al., 2011; Lin et al., 2016). The relationship between sediment strength and sonic velocity has previously been used to estimate the failure criteria parameters of both UCS and the coefficient of internal friction when cores are unavailable for direct laboratory testing (Chang, et al., 2006; Chang, et al., 2010). While sonic logs can be used to define a continuous strength profile, the sonic velocity derived strength parameters generally are calibrated to world wide data and are not field specific, particularly for sediments, which introduces additional uncertainty that can cause systematic overestimates of inferred stress state (Huffman et al., 2016). Thus, additional techniques are needed to determine sediment mechanical properties as a function of depth.

Early research in the petroleum and mining industries introduced the use of drilling parameter data to relate the response of a penetrating drill-bit to a measure of

rock strength (Bingham, 1964; Teale, 1965; Karasawa, et al., 2002; Ohno, et al., 2004; Kerkar, et al., 2014). Initial work in relating rock strength to drilling parameter data shows promising results; however, larger data sets are needed to confirm the estimates of rock strength and to further constrain the most applicable empirical relationships (Karasawa et al., 2002; Ohno et al, 2004). The use of drilling parameter data is advantageous because the data are routinely collected during all drilling operations. It is particularly valuable when core recovery or well logging data quality are poor, because in theory it can be used independently to determine a continuous log of rock strength over the length of a borehole.

The purpose of this work is to introduce a methodology for using drilling-parameter data acquired during IODP scientific drilling to determine sediment strength, with a focus on the strength of sediment with depth across the Nankai subduction zone. The Nankai subduction zone has been studied for many years through scientific drilling due to its history of naturally reoccurring tsunamigenic earthquake events, including the 1944 Tonankai (M8.1) and 1946 Nankaido (M8.3) events. Drilling data are readily available from IODP expeditions and can be used for geomechanical characterization of sediment strength. Under the International Ocean Discovery Program (IODP), a transect of scientific boreholes was drilled across the Nankai subduction zone to evaluate geomechanical properties of sediments both on the incoming plate and across the accretionary wedge. The methodology presented herein uses drilling parameter data to determine sediment strength profiles across the Nankai Trough Seismogenic Zone Experiment (NanTroSEIZE) transect to provide key information for stress analyses and

mechanics modeling, and to test hypotheses regarding strength variations associated with lithology, burial history, tectonic loading, and local faulting.

Project Objectives and Hypotheses

The overall objective of this study is to develop a methodology to determine sediment strength versus depth profiles from standard IODP drilling-parameter data and use the method to analyze data from the Nankai subduction zone to test the following hypotheses:

1. Within the depth range of scientific ocean drilling, sediments undergo rapid consolidation due to burial, dewatering and tectonic loading effects. Therefore, drilling response in marine sediments will change with depth and record a significant and non-linear increase in sediment strength as a function of increasing depth.
2. Sediment strength will increase landward across the Nankai subduction zone due to increased consolidation from horizontal tectonic loading within the prism relative to simple burial loading of sediments on the incoming tectonic plate.
3. With a sound characterization of the first-order variation in sediment strength with depth, which should be smoothly varying, the drilling-parameter data will provide a measure of second-order strength variations associated with faults and lithologic contacts.

CHAPTER II

GEOLOGIC BACKGROUND

The Nankai Trough reflects the subduction of the oceanic Philippine Sea Plate northwesterly under the Amurian Plate at approximately 58 mm per year (DeMets, Gordon, & Argus, 2010). A ~ 12 x 56 km 3D seismic survey captures the complex structure and stratigraphy over the NanTroSEIZE transect drilling sites analyzed for this project (Moore et al., 2007; Moore et al., 2009). The major morphotectonic zones identified by Moore et al. (2009) include the forearc Kumano Basin, the megasplay fault zone, the frontal thrust, and the Nankai Trench (Figure 1 and Figure 2).

The zones focused on in this work include the frontal thrust (Site C0006) and the hemipelagic sediment layer on the incoming plate (Site C0011). The frontal thrust is defined by a shallow dipping detachment that eventually runs parallel to bedding at its edge (Moore et al., 2009). The maximum horizontal stress trends NW for both the megasplay zone and the frontal thrust from borehole breakout analysis and suggests the overall stress magnitude is consistent with trench-normal shortening by thrusting and consolidation (Kinoshita M. et al., 2009b; Lin et al., 2016). As such, the sediments within the frontal thrust are representative of tectonically deformed and accreted sediments. Evaluation of borehole breakouts within the outer rise Shikoku Basin sediments suggests that stress state is in a normal faulting regime and that the maximum horizontal stress trends N-NE, oblique to the convergence direction of the Philippine Sea Plate (Saito et al., 2010). The sediments of the outer rise should be representative of

normally consolidated marine sediments, due to burial alone, that are entering the trench. Therefore, the greater degree of deformation of the frontal thrust relative to the outer rise provides the opportunity to test whether analysis of drilling-parameter data can characterize the different consolidation and sediment strength of sediment for the two different regimes.

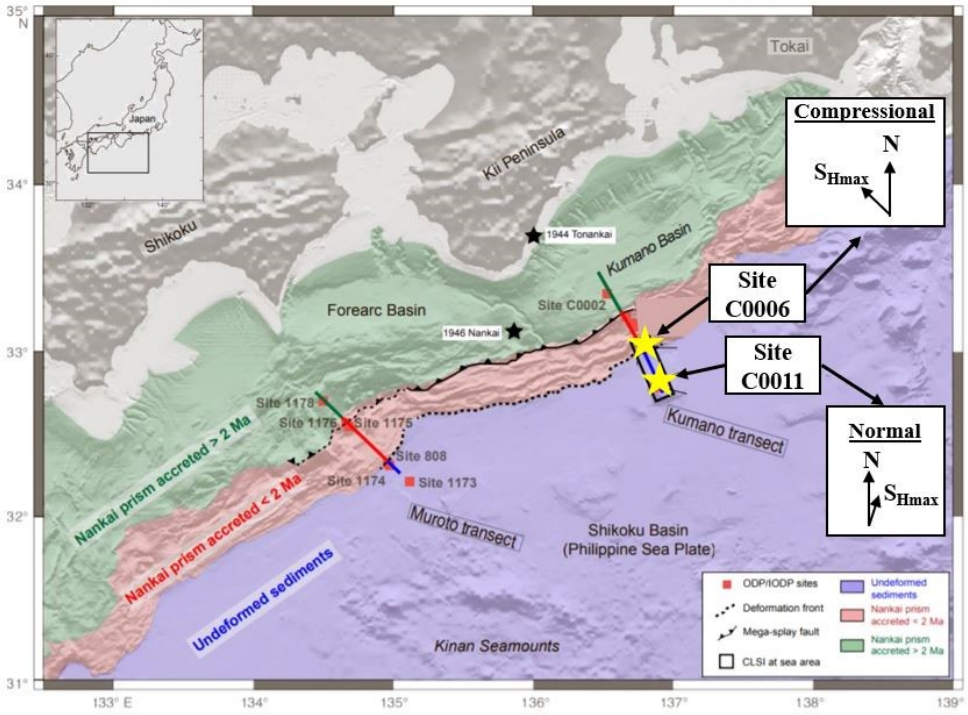

Figure 1 Map of the Nankai Trough showing the location of the IODP NanTroSEIZE transect and drill sites, and the in-situ stress directions, across the plate boundary**.** Site C0006 is located at the deformation front defined by a thrust stress regime. Site C0011 is within the outer rise Shikoku Basin sediments and demonstrates a normal faulting stress regime. Distribution of undeformed and accreted sediments are indicated by color shading. Adapted from Cerchiari et al. (2018).

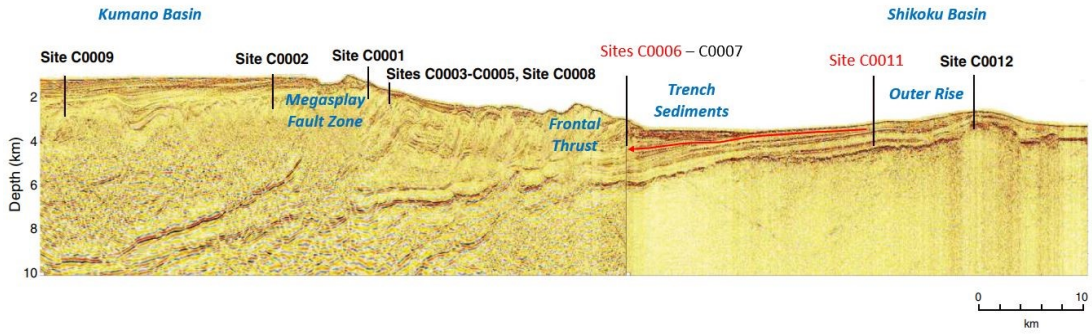

Figure 2 Seismic cross-section across the Nankai subduction zone showing the location of all Expedition drill sites (314/315/316 and 322) on the Kumano transect. Site C0006 is located on the hanging wall of the frontal thrust zone, while Site C0011 is within the outer-rise Shikoku Basin. Outer-rise sediments are actively subducting at the deformation front. Seismic images are from NanTroSEIZE landward of the trench and from the IFREE survey Line 95 seaward of the trench. Adapted from Henry et al. (2012).

IODP Drilling Site C0011

IODP Drilling Site C0011 is located within the outer rise sediments of the Shikoku Basin (Figure 1 and Figure 2). The primary purpose of drilling at that site was to characterize the sediments on the incoming plate prior to the initiation of deformation associated with subduction and the frontal thrust. Overall, the secondary structures observed within the cores are subtle, but consistent with subduction input sediments undergoing normal burial compaction and horizontal extension. The sedimentary section in this region consists of the following lithologic units determined from core analysis at Holes C0011B, C0011C, and C0011D (Saito et al., 2010; Henry et al., 2012):

- Unit I (0 – 340 m below sea floor, mbsf): Upper Shikoku Basin – hemipelagic/pyroclastic sediments

- Unit II (340 -479.06 mbsf) Middle Shikoku Basin – Silty claystone with tuffaceous/volcaniclastic sandstone
- Unit III (479.06 – 673.98 mbsf) Lower Shikoku Basin – Silty claystone
- Unit IV (673.98 – 849.95 mbsf) Lower Shikoku Basin – Tuffaceous silty claystone with silty sandstone turbidites
- Unit V (849.95 – 876.05 mbsf) Volcaniclastic-rich deposits – Tuffaceous sandy siltstone

The lithology is largely dominated by hemipelagic mud and claystone, with a large package of volcaniclastic sandstone within Unit II. The stratigraphic age begins within the Pliocene at Unit I to the middle Miocene at Unit V. Units II and III are presumed to have been deformed by a phase of sediment creep on the evidence of layer-parallel faults (Saito et al., 2010). As mentioned above, borehole breakout analysis suggests the maximum horizontal stress direction is N25°, oblique to the convergence direction of the Philippine Sea Plate (Saito et al., 2010). The extensional stress regime at Site C0011 suggests sediments have consolidated normally with burial depth or with reduced horizontal loading associated with extension.

IODP Drilling Site C0006

IODP Drilling Site C0006 is located at the toe of the accretionary prism (Figure 1 and Figure 2). The primary purpose of drilling at this site was to evaluate (1) the evolution of the frontal thrust, (2) how the frontal thrust relates to earthquakes, (3) and fluid, slip, and deformation interactions (Kinoshita M. et al., 2009a). Characteristic of a trench-perpendicular, horizontal shortening regime, Site C0006 is marked by reverse

shear deformation bands that strike NE (Kinoshita M. , et al., 2009a). The sedimentary section in this region consists of the following lithologic units determined from core analysis at Holes C0006F and C0006E (Kinoshita M. et al., 2009a), and logging-while-drilling (LWD) analysis at Hole C0006B (Kinoshita M. et al., 2009c).

- Unit I (0 – 27.23 mbsf): Trench to Slope Transition Facies
- Unit II (27.23 – 449.67 mbsf): Trench Deposits
    - Unit IIA (27.23 – 72.06 mbsf): Sand-Dominated Trench Wedge
    - Unit IIB (72.06 – 163.33 mbsf): Mixed Sand-Mud Trench Wedge
    - Unit IIC (163.33 – 391.33 mbsf): Mud-Dominated Trench Wedge
    - Unit IID (391.33 -449.67 mbsf): Mud Dominated Trench Transition
- Unit III (449.67 – 603.00 mbsf): Deep Marine Basin Muds with tuff layers
- LWD Unit IV (711.5 – 881 mbsf) Trench Complex Sands

Overall the section consists of shallow, sand dominated intervals above 164 mbsf, and progressively increases in hemipelagic mud sediments downward. Units I through IID are all Pleistocene in age, with Unit III ranging from Pleistocene to Miocene. Interbedded sands and ashy intervals are abundant, as well as repeated sequences of faults. LWD Hole C0006B provided evidence of trench complex sands in Unit IV that, due to poor core recovery, Hole C0006F was unable to document. The actual true stratigraphic thickness within these units is difficult to estimate due to the amount of repeated sequences from displacement on imbricate thrust faults (Kinoshita

M. et al., 2009a). The degree of deformation indicated by the localized imbricate thrusts supports the hypothesis that sediment response to drilling at Site C0006 will reflect an increase in sediment strength and overconsolidation due to the prevalent maximum horizonal stress acting as the maximum principal stress following Anderson's theory of faulting (Anderson, 1905). The upper Shikoku Basin sediments identified at Unit I within Site C0011 are correlated to Unit III of the deep marine basin sediments in C0006F, allowing the drilling data comparison between the same stratigraphic package at varying depths and stress regimes (Cerchiari et al., 2018).

CHAPTER III

DRILLING DATA AND SEDIMENT PROPERTIES

Drilling Operations

The NanTroSEIZE drilling operations utilize a rotary system controlled by a top drive (a hydraulic power swivel, HPS) that is directly connected to the drill string and the drill bit. A drill string, generally, is made up from top to bottom of drill pipe and a bottom-hole assembly (BHA). The BHA is further composed of several components specific to the operation and type of hole being drilled, but often includes heavy-weight drill collars (DC), logging tools, steering tools, and the bit itself. Drill collars are used primarily to help apply weight to the bit, while logging and steering tools help the drillers understand and control the direction of the bit. Advancement of the bit requires a normal force exerted at the bit, representing the total weight of the drill string less the load carried by the ship via the top drive, the buoyant force of the drill string in the fluid column, and the frictional forces of the drill string on the borehole walls. Torque then rotates the drill string. As the bit advances, new joints of drill-pipe are added to the drill string. The NanTroSEIZE expedition utilized several different specialized drill strings and BHAs to serve the different purposes of each scientific borehole. Generally, the expeditions ran 5.5”, 5.68”, or 5.75” S-140 or S-150 drill pipe and either a coring BHA or LWD BHA. Drillers observe a number of parameters in order to maintain borehole stability and maximum efficiency of drilling such as: well depth, weight on bit (WOB),

rotary speed (HPS Speed), rotary torque (HPS Torque), and rate of penetration (ROP) (Mitchell & Miska, 2011).

Performance at the bit is controlled by a variety of factors, the most relevant being bit properties, weight on bit, rotary speed, mud properties, and hydraulic properties. The bits used in LWD operation in Expeditions 314 were fixed cutter polycrystalline diamond compact (PDC) bits comprised of multiple fixed blades that rotate as a single unit (Kobayashi et al., 2008). PDC bits cut the sediment by shear failure and therefore require less WOB, or force, and higher rotational speeds to cut. WOB values have a direct impact on the lifespan of a bit as lower WOB dramatically reduces the bit wear, therefore increasing the efficiency of drilling operations (Mitchell & Miska, 2011). In addition to hydraulic piston coring, two other coring systems used in the expeditions are the Rotary Core Barrel (RCB) system or the Extended Shoe Coring System (ESCS). RCB is a coring system that utilizes a wireline-retrievable inner core barrel that is pumped down the inside of the drill string and latched into the BHA. The bit and BHA can then be rotated while the inner core barrel remains stationary via a system of bearings. In contrast, ESCS coring, also known as Extended Core Barrel (XCB) coring, allows for the recovery of core from softer sediments beyond the main BHA by the extension of a cutting shoe into the sediments ahead of the bit. Within harder formations, the cutting shoe is retracted to allow the RCB bit to operate (Baldauf et al., 2004).

Drilling fluids are a vital part of drilling operations as they can have profound impacts on the overall penetration rate at the bit (Mitchell & Miska, 2011). Mud weight

serves a number of purposes including transportation of cuttings and well-bore stability. In riserless drilling operations, the mud is pumped through the drill string to the bottom of the hole, through several orifices in the bit, and up through the annular space between the drill string and the borehole to the seafloor. Well-bore stability is achieved by using drilling mud to balance the formation pressure and preventing formation fluids from flowing into the well-bore. The riserless drilling operations in Expeditions 314/315/316 report the use of 5-10 m^3 of seawater gel slurry per stand, increasing to 10 m^3 per joint past 250 mbsf. During coring operations, less than 250 mbsf used 5m^3 per stand and then 10m^3 per half stand past 250 mbsf. Several times during operations, when hole conditions became poor either due to unremoved cuttings at the bit or insufficient annular fluid velocity, drilling ahead was temporarily halted for larger volume circulations of the sea water gel slurry used for drilling fluid until hole conditions improved. Expeditions 314/315/316 and 322 followed a similar mud weight program for all holes so mud weight is assumed not to have influenced drilling performance when comparing different holes (Kobayashi, et al., 2008; CDEX, 2010).

Specific Energy and Rock Relationships

Optimization of drilling operations has been heavily investigated due to its impact on cost efficiency in oil and mining industries, and has evolved into understanding the physical rock properties observed at the bit. Teale (1965) first suggests the relationship between drilling operations, maximum operation efficiency, and measurable rock strength. The rotary drilling process utilizes axial force (WOB) to initially “crush” or penetrate the rock and is measured normal to the rock interface and is

therefore not affected by any lateral forces. Torque is used to "cut" the rock surface as the bit is rotated laterally to break out fragments of the rock and is measured parallel to the rock interface.

To express the amount of energy required to excavate a unit volume of rock, Teale (1965) defines the parameter specific energy (E'_s) in kPa which is a function of the work done in both thrust and torque and is expressed by

Equation 1

$$E'_s = \frac{F}{A} + (\frac{2\pi}{A})\frac{NT}{u}$$

where A is the cross-sectional area of the bit in m^2, F is force or WOB in kN, u is penetration rate in meters/second, N is the rotary speed in revolutions/second and T is torque in kN-m. The rotational ($E'_{s\,T}$) and thrust ($E'_{s\,F}$) components are expressed in kPa by

Equation 2

$$E'_{s\,T} = (\frac{2\pi}{A})\frac{NT}{u}$$

Equation 3

$$E'_{s\,F} = \frac{F}{A}$$

Teale (1965) proposes that there will be some minimum value of energy to excavate a unit volume of rock that is entirely dependent on the rock strength. Therefore, the minimum value of specific energy ($E'_{s\,min}$) is deemed the maximum mechanical efficiency or the minimum amount of work required to excavate a volume of rock. Processes such as breaking the rock into smaller particle than necessary, friction loss between the rock and bit, and mechanical friction loss from drilling operations, result in

ambiguity between the actual and theoretical measurement of the maximum specific energy of the rock. Despite this, Teale (1965) suggests the specific energy and the compressive strength of rock must share a relationship as they are both a function of rock strength, and provides experimental evidence that minimum values of specific energy are correlated with measured values of compressive strength.

Performance Curve Analysis

The Drilling Performance Curve was developed by Bingham (1964) to understand the role of specific energy and maximize drilling operations for cost efficiency. Bingham (1964) presents the $\frac{u}{N}$ vs $\frac{F}{d}$ plot defined by the penetration rate (u) in meters/second, the rotary speed (N) in revolutions/second, bit diameter (d) in meters, and the bit load (F) in kilonewtons (Figure 3). The ratio $\frac{u}{N}$ represents the response of the work done on the bit in meters/revolution, while the ratio $\frac{F}{d}$ is used to represent the amount of axial energy required for input in kilonewtons of loading per meter. The linear portion of the $\frac{u}{N}$ vs $\frac{F}{d}$ plot (i.e., the drilling performance curve), is regarded as the conditions in which drilling performance is efficient and is used by drilling engineers to achieve the maximum penetration rate at the minimum power during drilling operations. Non-linear portions near small and large values of penetration rate represent the work lost due to friction (bit sliding without cutting) and bit-balling (additional friction because cuttings are not removed from the bit), respectfully. Based on this understanding, the expectation is that a "harder" rock will require more energy to drill and thus differences in rock strength will be reflected by the performance curve. The

linear portion of the performance curve (Figure 3) may be expressed approximately by the relation

Equation 4

$$\frac{u}{N} = \frac{a_F(F - F_c)}{d}$$

where a_F is the slope in m^2/kN and $\frac{F_c}{d}$ is the intercept value in kN/m for $\frac{u}{N} = 0$. The intercept value is determined from linear extrapolation of the maximum efficiency of the performance curve (i.e., linear portion), which effectively removes inefficiency associated with friction. (Bingham, 1964).

Bingham (1964) observes that a change in rock strength alters the intercept value $\frac{F_c}{d}$. To understand this observation, Bingham (1964) expresses rock strength as the critical shearing stress of the rock, and plots the intercept value $\frac{F_c}{d}$ versus independent measures of rock strength for various rock types. The relationship between the critical shearing strength and rock strength is linear and thus, Bingham (1964) first identifies the relationship between rock strength and the axial drilling performance curve.

Following Bingham (1964) and Teale (1965), Karasawa et al. (2002) evaluate the drilling parameter approach by including torque (T) in kN-m to describe the rotational work done during drilling. Torque is related to the bit diameter using an altered theoretical energy equation by Warren (1984) expressed as

Equation 5

$$\frac{1}{\eta} A E'_{s\,min} u = Fu + 2\pi NT$$

where $E'_{s\,min}$ is the minimum specific energy assuming the thrust work is negligible ($E'_{s\,min} = \frac{2\pi NT}{Au}$) from Teale (1964), η is the bit efficiency factor, and area (A) is equal to $\frac{\pi d^2}{4}$ (Warren, 1984).

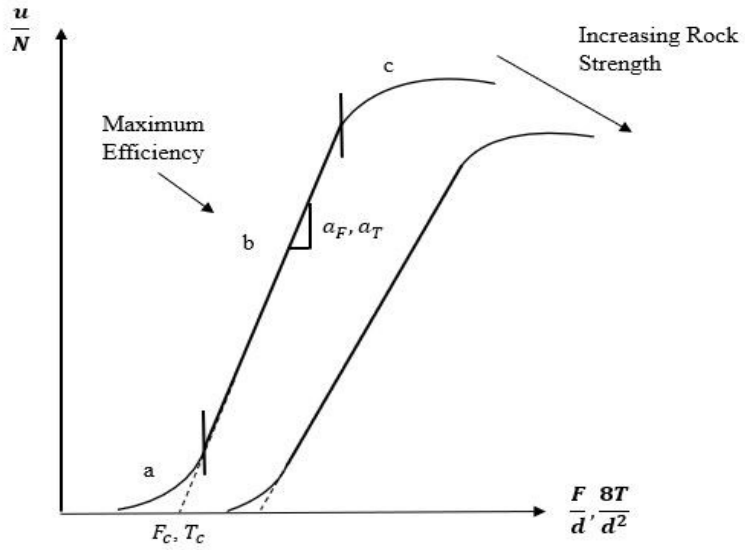

Figure 3 Schematic of the drilling performance curve for both axial ($\frac{F}{d}$) and rotational ($\frac{8T}{d^2}$) components. Non-linear sections a and c mark inefficient drilling due to the transition of scraping/grinding into shearing and bit foundering, respectively. Zone b is the area of drilling efficiency, termed the Performance Curve, with the maximum efficiency within the linear portion. Drilling parameters threshold (F_c and T_c) and slope (a_F, a_T) will increase and decrease, respectively, with increase in rock strength.

Equation 5 is rearranged to solve for $\frac{u}{N}$ so that torque is related to the bit diameter (d) by $\frac{8T}{d^2}$ as the rotary energy per revolution divided by the cross-sectional area of the bit. This is expressed as

Equation 6

$$\frac{u}{N} = \left(\frac{\eta}{E'_s}\right)\left(\frac{2\pi T}{\frac{\pi d^2}{4}}\right) = \left(\frac{\eta}{E'_s}\right)\left(\frac{8T}{d^2}\right)$$

where the area $\mathrm{A} = \frac{\pi \mathrm{d}^2}{4}$. As presented by Teale (1965), $E'_{s\,min}$ is then equated as the unconfined compressive strength of the rock.

Similar to Equation 4, the relationship for the rotational component of specific energy within the performance region may be expressed with the linear relationship

Equation 7

$$\frac{u}{N} = a_T \frac{8(T - T_c)}{d^2}$$

where a_T is the slope of the performance curve in m^2/kN and $\frac{8T_c}{d^2}$ is the slope intercept in kN/m for $\frac{u}{N} = 0$. The intercepts of both Equation 4 and Equation 7 are deemed to represent the threshold values at which tooth penetration commences for threshold weight (F_c) in kN/m and threshold torque (T_c) in kN/m (Figure 3). The combination of the $\frac{u}{N}$- vs $\frac{F}{d}$ and $\frac{u}{N}$- vs $\frac{8T}{d^2}$ plots represent the total work done by the bit by both axial (thrust) and rotational (torque) energy. With both theoretical work components accounted for, the estimation of rock strength may be expressed as

Equation 8

$$\left(\frac{8(T - T_c)}{d^2}\right)^2 = \left(\frac{a_F}{{a_T}^2}\right) \frac{(F - F_c)u}{Nd}$$

where the slopes a_F and a_T depend on rock strength and bit wear.

In summary, Bingham (1964) and Karasawa et al. (2002) present possible mathematical solutions to predict rock strength from drilling parameter data. Other researchers have also expanded on this theory, creating further relationships between drilling parameter data and rock strength (Ohno et al. 2004; Kerkar, 2014; Shi 2015; Huffman, 2016; Hamada et al., 2018). However, the mathematical solutions presented require large, field-based data to test the applicability of the various solutions presented to best utilize drilling parameter data as a method to measure rock strength, which has been done extensively in the petroleum industry, but not for IODP scientific drilling in marine sediments. The methodology discussed in the following chapters addresses the processing of field drilling-parameter data and how it is applied to evaluate the relationship between the response of the bit to sediments and sediment strength by exploring the solutions expanded by Bingham (1964) and Karasawa et al. (2002).

CHAPTER IV

PERFORMANCE CURVE ANALYSIS OF SITE C0006

Available Data

The drilling data for this analysis were made available to members of the science party while on board the D/V Chikyu during the Expeditions 314, 315, 316, 322 and 338 (personal communication, F. M. Chester and H. Kitajima, 2017), which include raw drilling-parameter data. In addition, the daily drilling reports and the CDEX Technical Report, 2007-2008 Drilling Completion Report NanTroSEIZE Stage 1, provided supporting information such as drill-bit information (type, diameter) and general drilling operations and setbacks for each drill hole.

Scientific data and additional information for these expeditions is available from http://sio7.jamstec.go.jp/, a server designated to distribute all available data from D/V Chikyu that is operated by the Center for Deep Exploration (CDEX) and Japan Agency for Marine-Earth Science and Technology (JAMSTEC). Information acquired from this site and used for this research included LWD data (gamma ray, resistivity, sonic, etc.), coring descriptions and images, and other geophysical and geomechanical data.

Data Processing

Analysis of the raw drilling data utilized the following main drilling parameters: Bit Depth in meters, Total Depth in meters, HPS Speed in rev/min, HPS Torque in kN.m, pump rate in Active Strokes per Minutes (SPM), and Weight on Bit (WOB) in kN (Figure 4). Ideally, WOB and HPS Torque are measured downhole at the bit, as opposed

to the available surface measurements, to mitigate inaccurate measurements of the drilling data due to frictional loss from the drill string. For shallow, non-riser holes drilled during these IODP expeditions we use the only available data (surface data) and assume the frictional loss is small and relatively similar from hole to hole, and can be ignored for comparative studies. During drilling operations, the data generally is collected at 1 Hz but reported only at a timed sampling rate ranging from 10 seconds to one minute depending on the drill hole. The sampling rate had a direct impact on the quality of data analysis as the data sets sampling at rates greater than 20 seconds were very difficult to accurately model or analyze. As such, much of the data analysis herein is restricted to data sets with sampling rates at 0.1 Hz.

Rate of Penetration (ROP) in m/s is an important parameter this is not always calculated or reported the same from well to well. To remain consistent, the ROP is calculated for each data set by dividing the change in depth by the change in time when the bit advances. The result is a ROP value that is not time-indexed to the individual instantaneous measurements. To index the calculated ROP and the other measured drilling parameters, the other measured drilling parameter values are averaged for every two consecutive values to produce a single value representing a similar time interval as the ROP, and thus both smoothing and indexing the entire data set. In assessing the data, averaging intervals larger than two consecutive indices resulted in overly smoothed data values that do not preserve significant signals in the raw data.

After the drilling parameters are properly averaged and determined, the data are filtered to retain data only for the case if the bit advanced, i.e., actively cut into the

sediment and lengthening the drill hole. This is accomplished by determining the indices for which the Bit Depth is approximately equal to the Total Depth. The data are further filtered for indices with both ROP and HPS Speed greater than zero. The filtering effectively removes data associated with returns on coring runs or re-tracking of the bit, and as such only includes information for when the bit was interacting with sediment.

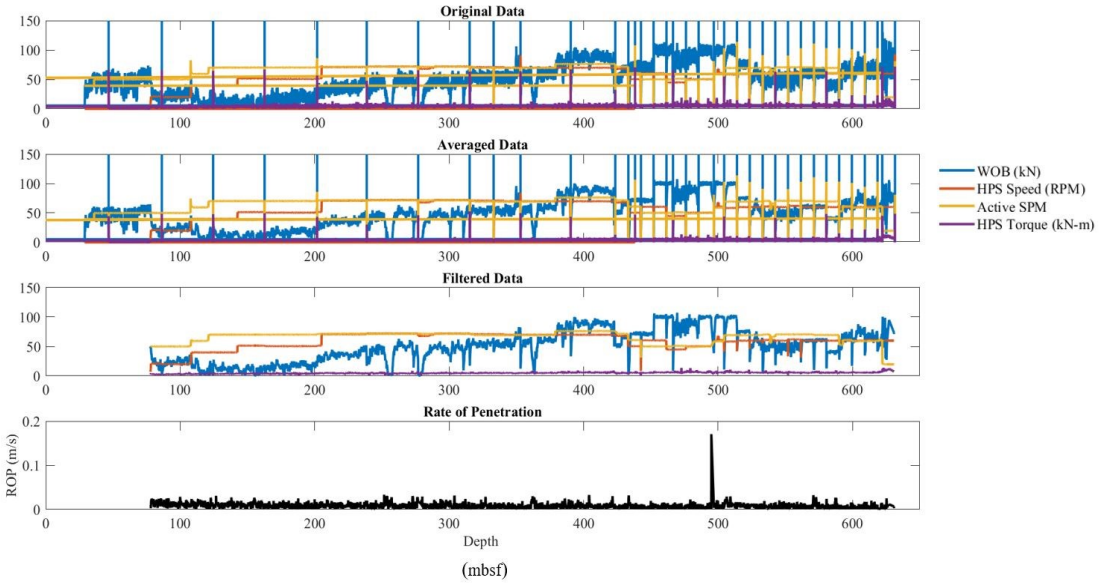

Figure 4 Example of raw and processed drilling data from Hole C0006F. Large vertical deviations in the data (e.g., WOB) in both the Original and Averaged Data reflect the bit running up and down the hole. Filtered Data shows the result of processing and filtering to retain only the data for when the bit is advancing through sediment, i.e., deepening the hole. ROP is calculated from the change in distance divided by the change in time in meters/second.

Performance Curve Analysis

The drilling data are analyzed in terms of the performance curve by plotting the penetration rate ($\frac{u}{N}$) in m/revolution versus the thrust energy ($\frac{F}{d}$) in kN/m, and versus the rotational energy ($\frac{8T}{d^2}$) in kN/m. The energy terms are expressed in terms of *d*, bit diameter; however, several types of bits are employed in drilling IODP boreholes. For LWD boreholes, the bit diameter is equivalent to the outer diameter because there is no hole for coring. For operations employing a rotary core barrel (RCB) bit containing a coring hole, a center bit initially is inserted for drilling to the desired depth before initiating coring by removing the center bit. Therefore, the bit diameter is equated to the outer diameter if the center bit is inserted, but by the difference between the outer diameter and the inner diameter if the center bit is removed for coring. With the different bit diameters defined, the variables for the $\frac{u}{N}$ vs $\frac{F}{d}$ and $\frac{u}{N}$ vs $\frac{8T}{d^2}$ plots are calculated by the following relationships:

Equation 9

$$\frac{u}{N} = \frac{60*ROP}{HPS\ Speed}, \frac{F}{d} = \frac{WOB}{d_O - d_I}, \text{ and } \frac{8T}{d^2} = \frac{8*HPS\ Torque}{{d_O}^2 - {d_I}^2}.$$

The data are binned into depth intervals to represent the drilling response as a function of depth; the depth interval employed is 5 m because smaller intervals had insufficient data and larger intervals resulted in lower resolution. Binning data facilitates documenting how the performance curve intercept and slope change with depth. Due to the filtering process, some of the depth intervals do not have sufficient data to define a linear fit to the performance (2 points or less) and are therefore omitted from further processing.

With the data binned to 5 m depth intervals, a linear relationship is determined for both $\frac{u}{N}$ to $\frac{F}{d}$ and $\frac{u}{N}$ to $\frac{8T}{d^2}$ for each depth interval. To best match the performance curve fitting presented by Bingham (1964) and Karasawa et al. (2002) for experimental drilling data (which is high quality), the linear fitting of the binned data are carried out after determining an initial threshold (intercept) torque and force for each depth interval (Figure 5). After many trials, the following approaches were adopted to determine the threshold. For the $\frac{u}{N}$ to $\frac{8T}{d^2}$ data intervals, the threshold torque is calculated as the mean of the data from the lowest 10th percentile of the rotational energy ($\frac{8T}{d^2}_{10\%\ trq\ bit}$). For the $\frac{u}{N}$ to $\frac{F}{d}$ data intervals, the threshold thrust also is calculated from the indexes corresponding to the mean of the lowest 10th percentile of the rotational energy ($\frac{8T}{d^2}_{10\%\ trq\ bit}$). Fitting the linear relationship to the binned data are constrained by the calculated threshold value with the slope is determined through least-squares fitting. Although both Bingham (1964) and Karasawa et al. (2002) suggest that the threshold intercept values should be determined at a penetration rate of zero, such a determination for the IODP drilling data often resulted in an unphysical negative value because the field-based data are collected under conditions not as ideal as the experimental data, and penetration rate values may be artificially shifted positive due the data filtering methodology. Accordingly, the calculated mean threshold value as defined above is assumed equal to the true intercept value.

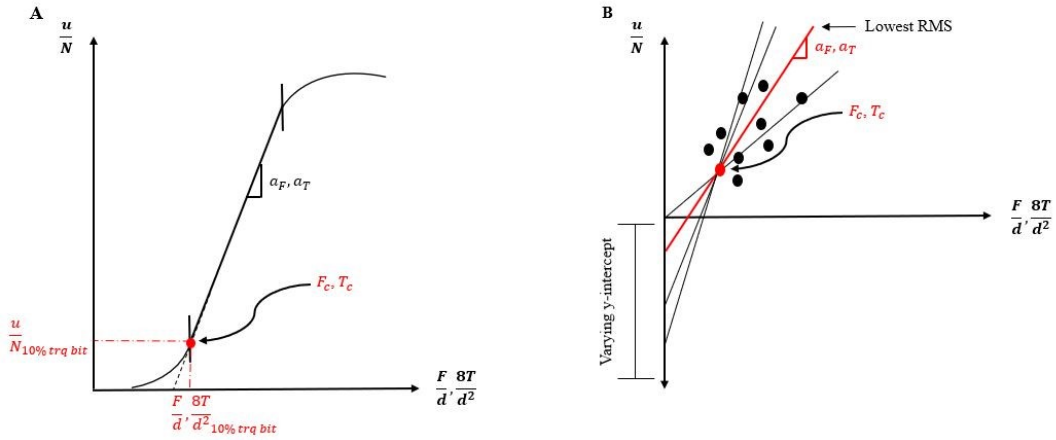

Figure 5 A) Schematic plots illustrating the determination of the threshold and slope of the performance curve. **B**) Schematic of the slope evaluation process for each depth interval of data (see text for explanation).

For each depth interval, the threshold value of $\frac{F}{d}$ and $\frac{8T}{d^2}$ are used to calculate many possible slopes of a linear performance curve (for a_F and a_T) containing the threshold value by assuming 5000 negative $\frac{u}{N}$ values (y-intercept value) ranging from zero to -3 (Figure 5). For each y-intercept value, the goodness of fit (RMS) is determined, and the slope with the lowest RMS value is selected as the best fit slope for the performance curve at that depth interval. From this determination for all depth intervals, the slopes and intercepts of the best fit performance curves may be plotted against depth to capture the change in sediment response to drilling with depth.

Example Analysis of Drilling Data for Site C0006, Hole F

The methodology above is applied to Hole C0006F, which was drilled during IODP Expedition 316, at a water depth of 3875.5 m and a spud date of January 7, 2008.

The bottom-hole assembly (BHA) consisted of a rotary core barrel (RCB) with a bit outer diameter of 9-7/8 in (250.83 mm) and inner diameter of 2-5/16 in (58.74 mm). Drilling with a center bit continued until 395 mbsf, where the center bit was retrieved and coring operations began, until 603 mbsf when deteriorating hole conditions led the drillers to abandon the hole on January 13, 2008. Overall, the coring recovered 23 cores at a 27.15% average recovery rate for a total of 56.48 m (Kinoshita M. et al., 2009a).

After filtering the drilling data and calculation of the penetration rate ($\frac{u}{N}$) and axial and rotational energy components ($\frac{F}{d}$ and $\frac{8T}{d^2}$), the data are plotted in performance space and color-coded according to the associated depth intervals (Figure 6). The plots clearly show that the data for each lithologic unit (and depth interval) are clustered consistent with changing sediment response, and with an overall increase in threshold and decrease in slope of performance with increasing depth as expected for a sedimentary section.

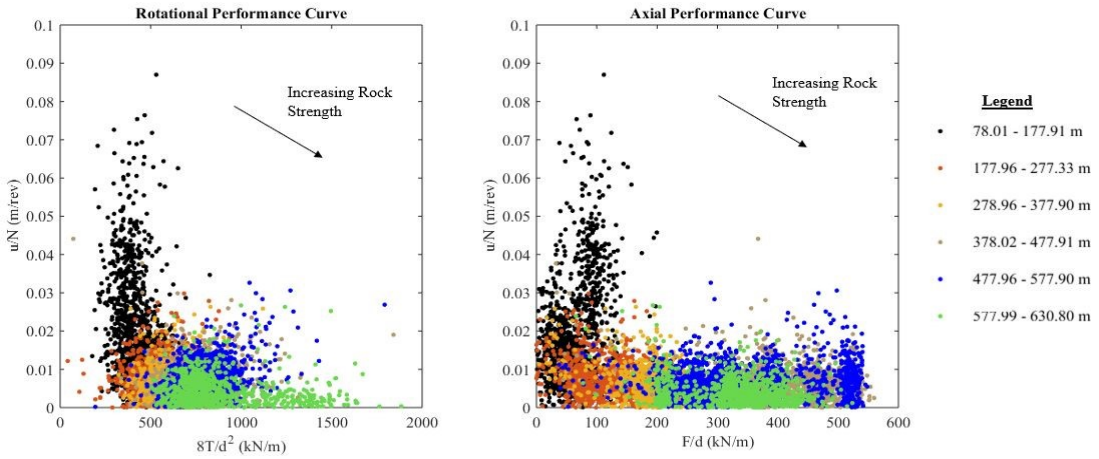

Figure 6 Drilling-performance parameters for Hole C0006F plotted in performance space. Data are color-coded for 100 m depth intervals to illustrate overall depth-dependence of drilling performance. Qualitatively, comparing performance data associated with each depth interval shows that the threshold values increase and the slope decreases with increasing depth as expected for sediments.

The results of fitting performance curves to the binned, 5-m interval data sets for Hole C0006F are illustrated by plotting threshold and slope values as a function of depth (Figure 7). The plots show a systematic change in the slope and threshold values of fitted performance curves with depth for both the rotational (torque) and axial (force) data consistent with a non-linear increase in sediment strength with depth. For this example, the performance parameters (threshold and slope) show somewhat more variability in axial then rotational energy. The plots of performance parameters also indicate goodness of linear fits to the depth-interval binned data sets in terms of the RMS value associated with the best-fit slope (Figure 7). Overall, the shallow intervals, less than 100 mbsf, show more variability in slope and higher RMS values than the deeper intervals. The

lithologic log for Hole C0006F (Figure 7) is used to compare the performance parameters to the associated lithologic units and identified faulting from core descriptions. There are some significant deviations from the overall trends likely reflecting changes in lithology (sands versus muds) and presence of faults indicated by core description and LWD analysis.

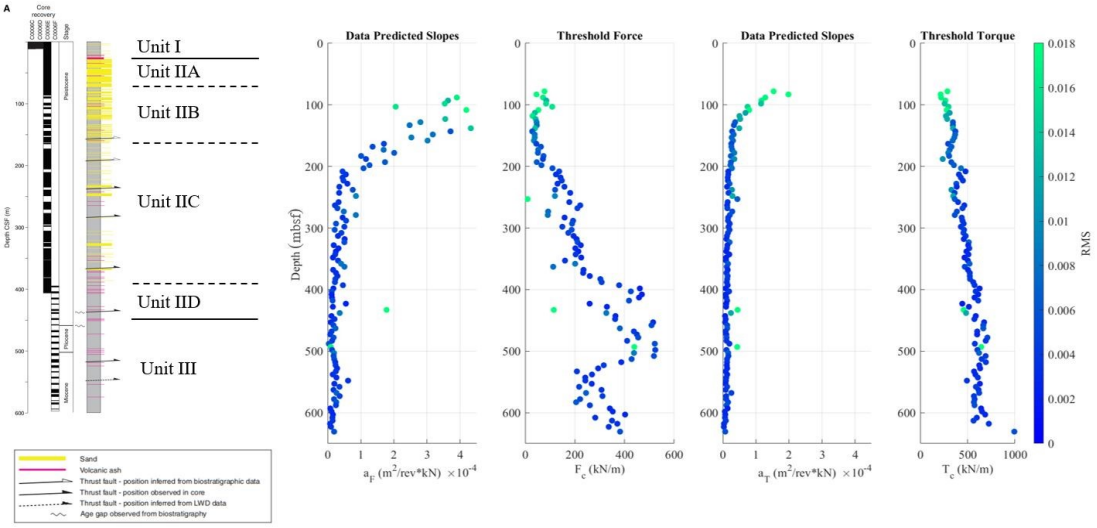

Figure 7 Comparison of threshold and slope values of the performance curves for axial and rotation energy as a function of depth, and with lithology, for Hole C0006F. Values are color coded by the RMS value associated with the best picked slope to represent how well the slope and threshold predict the drilling performance data for each 5-meter depth interval. Overall, the threshold values increase with depth, and the slopes decrease with depth. Comparison to Site C0006 lithology shows correlation of data outliers with thick sand layers and noted thrust faults (e.g., 240-250 mbsf). Lithologic unit chart adapted from Kinoshita M. et al. (2009a).

CHAPTER V

DRILLING PERFORMANCE MODEL FOR SEDIMENT CONSOLIDATION WITH DEPTH

Marine sedimentary deposits generally display a reduction in porosity with depth associated with physical processes of consolidation driven by loading from the sedimentary overburden and accommodated by the expulsion of pore fluids. The relationship between sediment strength, porosity, overburden, lateral confinement, and depth of burial has been studied extensively in the geotechnical civil engineering field (Wood, 1990; Terzaghi et al., 1996; Holtz et al., 2011) and in the geophysical rock mechanics field concerned with sediments and sedimentary rock (Wong et al., 1997; Karig & Morgan, 1994; Karig & Ask, 2003; Kitajima et al., 2012).

Geotechnical and geophysical studies document that during progressive burial of sediments the porosity decreases roughly proportional to change in the logarithm of the overburden stress. Overburden stress increases approximately linearly with burial depth, so the porosity - depth relationship should, to first order, follow an exponential form, which is generally observed (e.g., Athy, 1930; Bahr et al., 2001). In addition, for the case of progressive burial of sediment, the sediment is essentially always at yield; thus, the strength of the sediment is the same as the overburden and to first order is proportional to depth. There are a number of factors that further influence sediment consolidation and strength, such as composition and texture (lithology) of the sediments, secondary deformation such as by faulting and fracturing, and tectonic loading that can increase or

decrease the magnitude of mean stress relative to that typically assumed for normal consolidation in a basin, i.e., from overburden stress with an assumption of zero lateral strain.

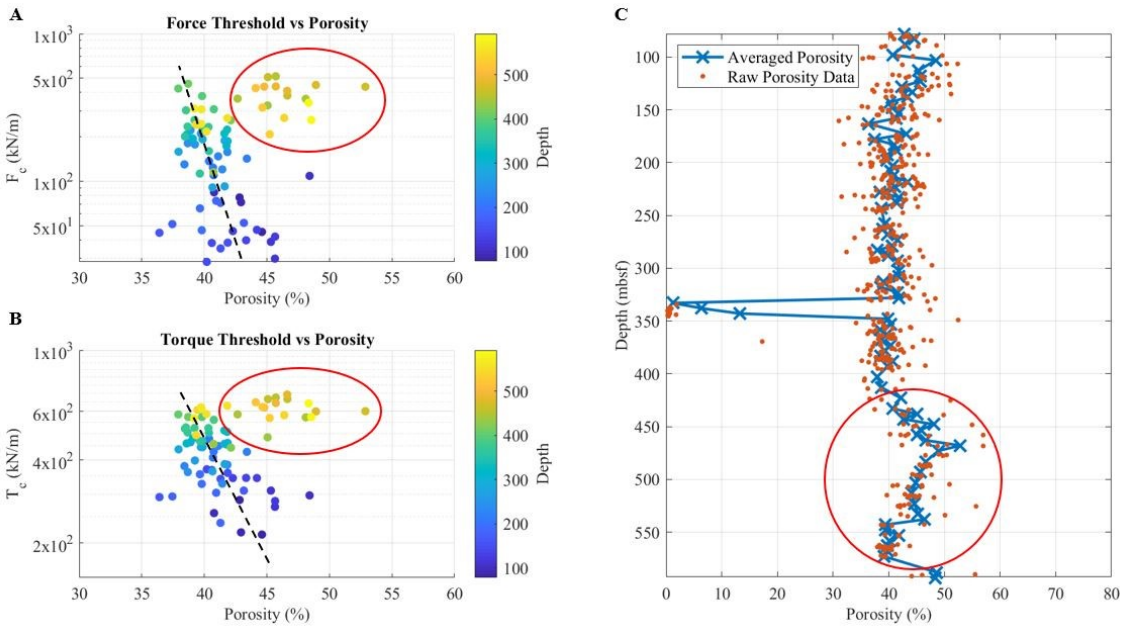

Figure 8 Plots showing the depth-dependent correlation between porosity and the threshold strength of sediments determined from drilling performance curves for Hole C0006F. Comparison of force (**A**) and torque (**B**) threshold values from Hole C0006F and the core-derived porosity from boreholes at Site C0006. Values are colored by depth (mbsf). Overall, there is an approximately linear correlation between threshold value and porosity with the exception of the clustering of data related to depths 425-550 mbsf (red circle). (**C**) Raw porosity data (orange) from core measurements and averaged porosity (blue).

The anticipated depth-dependent correlation between porosity and the strength of sediments determined from drilling performance curves may be tested by plotting porosity versus both the axial (F_c) and rotational (T_c) performance curve intercepts. From the general relationships noted above, porosity should decrease linearly with logarithm of strength (the performance curve intercepts), which is supported by observation (Figure 8).

Overall, the threshold values increase logarithmically with a decrease in porosity (Figure 8). An anomalous scattering of points highlights a high porosity zone (~50%) and increased threshold values in both force and torque (but particularly in Force) between 400 and 550 mbsf. This deviation from the overall trend with depth for both porosity and threshold values is discussed in Chapter VII.

On the basis of the general relationships and supporting observations of porosity and strength, and performance parameters, with depth, Chester & Kitajima (written communication, 2018) proposed functions for fitting the performance curves of drilling marine sediments, which can be used to describe the first-order changes in mechanical properties of sediments from consolidation associated with burial. Specifically, the intercept and slope parameters of performance curves are expressed with logarithmic and exponential functions of depth, respectively. The intercept of the performance curve for both the axial (F_c) and rotational (T_c) energy components as a function of depth is given by

Equation 10

$$F_c, T_{c_{model}}(z) = a + b * \log(c * z + 1)$$

where z is depth in meters, a, b and c are coefficients determined by fitting data. Coefficients a and b are in units of kN/m, and c in units of 1/m. The slope of the performance curve for both the thrust (a_F) and rotational (a_T) energy components as a function of depth is given by

Equation 11

$$a_F, a_{T_{model}}(z) = d + e * exp^{f*z+g}$$

where z is depth in meters, and d, e, f and g are coefficients determined by fitting data. Coefficients d and e are in units of m^2/kN, f in 1/m, and g is unitless.

A MATLAB curve-fitting application (Curve Fitting) is used to determine the coefficients of Equation 10 and Equation 11 that best-fit the slope and intercept values as a function of depth (Figure 9). Attempts to determine coefficient values from the slope and intercept values, irrespective of the influence of sediment composition (sand versus mud) and presence of fracture and fault zones on sediment strength, led to failed or unsatisfactory fits. Accordingly, a data weighting scheme was used to minimize the effects of data outliers associated with large intervals of porous sands and fracture/fault zones so that the model fits would represent the first order depth-dependence of strength for the dominant lithology, i.e., muds and clayey sediments. On the basis of shipboard data available for Site C0006 (Kinoshita M. et al., 2009a), primarily the visual core descriptions and other physical property measurements (e.g., natural gamma ray logs), the slope and intercept values from depth intervals characterized as zones of sand and of fracture and faulting are assigned a weighting factor of 2 and 5, respectfully, while the remaining depth intervals comprised of high mud and clay content are assigned a

maximum weighting factor of 10. This weighting leads to acceptable model fits which can be taken as representative of the overall depth-dependent strength of the mud sediments due to burial plus tectonic consolidation at Site C0006. The best-fit coefficient values are presented in Table 1 and Table 2.

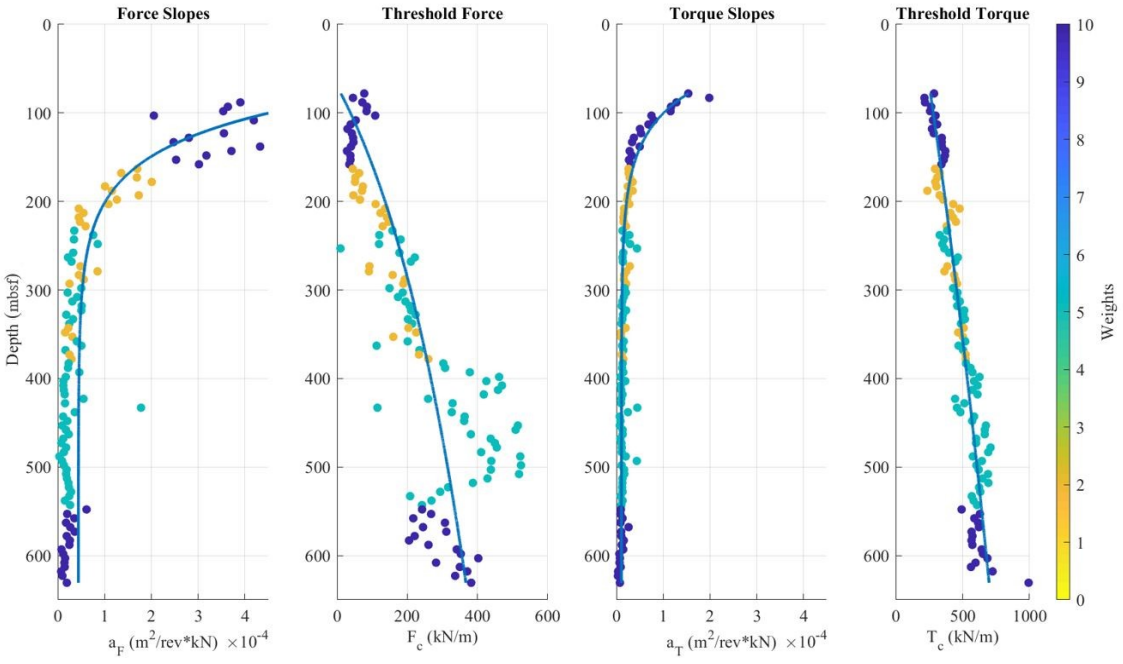

Figure 9 The marine-sediment, depth-dependent model fit to observed performance-curve threshold and slope data for Hole C0006F. Colors indicate data-weighting factors of 2 for sands, 5 for faults, and 10 for muds (see text). Overall, the functional forms of the model (blue line) fit the threshold and slope data well and represent to first order the overall trends of the data.

Table 1 Hole C0006F model coefficients and associated goodness of fit (R^2) for threshold values.

	a (kN/m)	*b* (kN/m)	*c* (1/m)	R^2
$F_{c_{model}}$	-115.80	278.80	0.0074	0.65
$T_{c_{model}}$	182.50	1164.00	0.00088	0.79

Table 2 Hole C0006F model coefficients and associated goodness of fit (R^2) for slope values.

	d (m^2/kN)	*e* (m^2/kN)	*f* (1/m)	*g* (.)	R^2
$a_{F_{model}}$	4.42E-05	0.0029	-0.020	-3.75E-07	0.72
$a_{T_{model}}$	1.09E-05	0.00074	-0.021	1.28E-07	0.90

CHAPTER VI

RELATIVE DRILLABILTY – CORRECTING FOR DEPTH

The drilling performance model captures the overall change in strength of sediment with depth reflected by drilling performance parameters. Accordingly, the model best-fit to drilling data for a site can provide a means to document and investigate local variations in drilling performance relative to the model, which may reflect other factors that dictate sediment mechanical properties at the site, such as variation in composition and texture associated with stratigraphic layering, fluid pressure, and secondary structures associated with fracture and faulting. In addition, the drilling performance model from one site may be compared to drilling performance at another site to document differences in the overall depth-dependence of sediment strength associated with lateral variation in tectonic loading or lithostratigraphy.

Relative Drillability is introduced herein to document the deviation of the local drilling performance from that predicted by a drilling performance model. The deviation of the model from the data, $Relative\ Drillability_{F,T}$, is defined as the difference (measured normal to the performance curve) between the observed performance data and the model performance curve for equivalent depth by the following relationship:

Equation 12

$$Relative\ Drillability_{F,T} =$$

$$[(\frac{F}{d_{obs}}, \frac{8T}{d^2}_{obs} - \frac{\left(\frac{u}{N_{obs}} - \frac{u}{N}_{10\%\ trq\ bit}\right)}{a_F, a_{T_{model}}} - F_c, T_{c_{model}}) * \sin(\tan^{-1}(a_F, a_{T_{model}}))$$

where $\frac{F}{d}_{obs}$, $\frac{8T}{d^2}_{obs}$ and $\frac{u}{N}_{obs}$ are the filtered and smoothed observed parameters from the well site of interest and $F_c, T_{c_{model}}$, $a_F, a_{T_{model}}$ and $\frac{u}{N}_{10\%\ trq\ bit}$ are the performance curve parameters from the drilling performance model **(**Figure 10). A plot of relative drillability as a function of depth for a borehole is analogous to a geophysics well-log, graphically illustrating the sediment response to drilling.

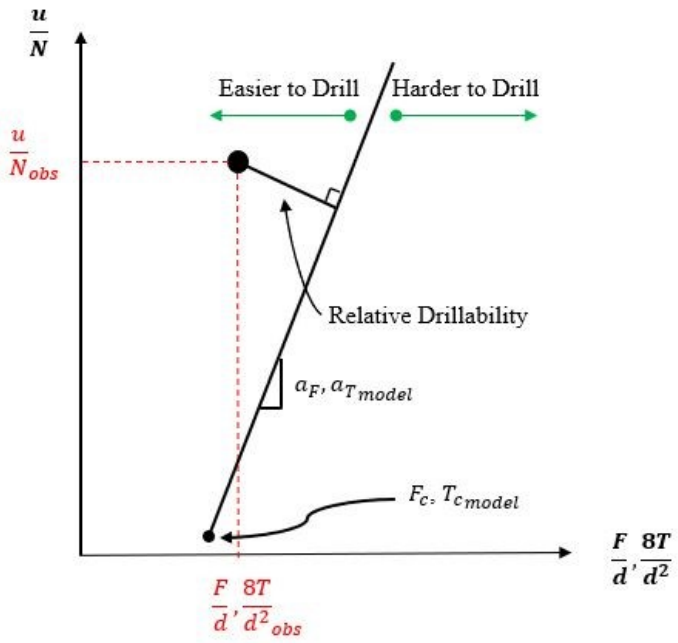

Figure 10 Schematic plot of the model performance curve and observed performance for a specific depth interval to illustrate the determination of Relative Drillability. The performance line for a specific depth is predicted by model parameters ($a_F, a_{T_{model}}$ and F_c, $T_{c_{model}}$). Relative Drillability is calculated by comparing the model to observed performance data $\frac{u}{N_{obs}}$ and , at each depth interval, and quantifies the local difference in actual sediment response from the expected overall depth-dependent response (easier or harder to drill) for the dominant lithology, i.e., muds and clayey sediments.

The $Relative\ Drillability_{F,T}$ is a residual value represented in plots versus depth by deflections of the curve to the left and to the right of zero, highlighting deviation from the performance model (represented by the gridline at zero). Deviations to the left are considered "weaker sediments that are easier to drill" (higher drillability) and deviations to the right are considered "stronger sediments that are harder to drill" (lower drillability), relative to the model that represents the depth-dependent response of the dominant lithology, i.e., muds and clayey sediments (Figure 10).

Comparison of the force and the torque relative drillability curves for Hole C0006F using the Hole C0006F reference model show good correlation, that is similar depths of deviation to the left and right (Figure 11). The most pronounced deviations to the left, which represent easier to drill, correlate with thicker sand layers which, from drilling experience, are more easily drilled than the finer-grained mud and clay-rich sediments. The overall position of the Relative Drillability curves for C0006F do not directly follow the model and shift slightly right of the model (i.e., slightly positive). This shift reflects the best-fitting procedure that employed a weighting process to emphasize fitting to the stronger, dominant fine-grained sediment component and de-emphasize the weight of the weaker sands and fractured sediment, but the effect of the weaker sediments is not completely removed, so the relative drillability of the dominant sediment is shifted slightly right.

The interval of 400 to 500 mbsf within the Unit IID and the upper portion of Unit III approaching 0 on the residual model suggesting it is easier to drill than the overlying sediments. This observation is supported by the significant increase in measured core

porosity, indicating a decrease in rock strength. As discussed later (Chapter VII), this zone was identified as having high fault damage and evidence of over pressure. Further experimental work is required to constrain the absolute value of model deviations and empirically relate the model to sediment strength.

Comparison of the relative drillability of both coring Hole C0006E and the LWD Hole C0006B to the RCB Hole C0006F using the C0006F reference model shows good consistency but also highlights some differences due to the different coring and logging operations. Hole C0006E implemented hydraulic piston coring systems (HPCS) and extended shoe coring system (ESCS) as opposed to the RCB system used in Hole C0006F (Kinoshita M. et al., 2009a). Water depth was determined on December 28, 2007 at 3877.5 mbsl, with HPCS running for the first 83.54 mbsf. ESCS, with an outer dimeter of 11-7/16 inches (290.51 mm), was then run to a total depth of 409.4 mbsf on January 6, 2008. Core recovery was 80.68% in average with a total length of 409.4 m. Hole C0006B was a LWD hole drilled as part of Expedition 314, and penetrated 885.5 m below the seafloor using a 8-½ inch (215.90 mm) LWD bit (Kinoshita M. et al., 2009c). All three holes at Site C0006 are within ~50 m from each other, so the sediment properties should not significantly different between the holes; however, there is significant thrust faulting that produces unit duplication and places the same stratigraphic and structural features at different depths in the different holes.

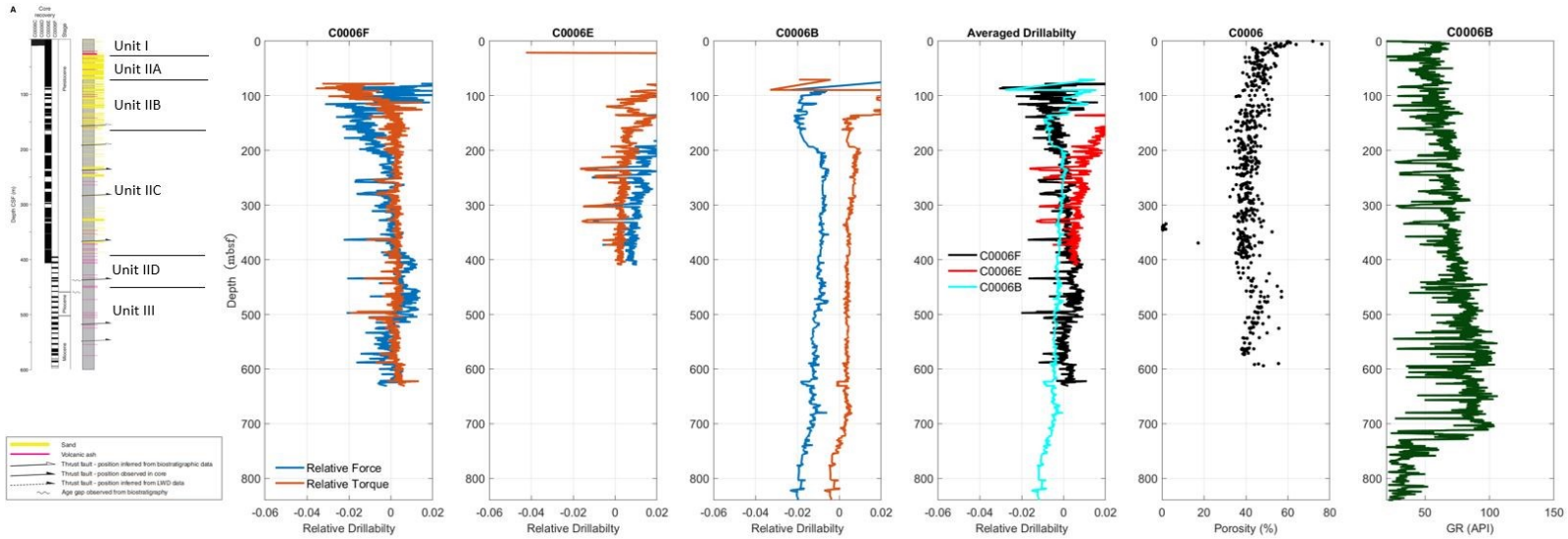

Figure 11 Comparison of Relative Drillability versus depth plots, and to lithology, for coring Holes C0006F, C0006E, and LWD Hole C0006B based on the Hole C0006F model. Deviations to the left signify "easier to drill" sediments than C0006F, and deviations to the right "harder to drill". For Coring Hole C0006E, Relative Drillability for torque aligns with the residual zero below 200 mbsf, similar to Hole C0006F; however, the Relative Drillability for force is overall more positive (harder to drill) than C0006F, which is most likely due to differences in coring systems (ESCS vs RCB). Deviations to the left in Holes C0006F and C0006E are correlated to thrust faults and sand intervals (240, 375, and 430 mbsf). LWD Hole C0006B shows little deviation until 700 mbsf where a strong deviation to the left is correlated with a thrust fault with trench channel sands in the footwall. Lithologic unit chart adapted from Kinoshita M. et al. (2009a).

In order to determine the Relative Drillability of Holes C0006E and C0006B using Hole C0006F as a reference model, the difference in drill bit sizes must be treated. The reference model derived from Hole C0006F is based on two different bit sizes reported for RCB drilling and RCB coring intervals. Therefore, a normalization for different bit size must be applied to $F_c, T_{c_{model}}$ and $a_F, a_{T_{model}}$, which was derived from unit analysis. The following is an example of applying the C0006F model to observation in Hole C0006E:

Equation 13

$$T_{c_{model-C0006E}} = \frac{8To}{d^2{}_{C0006F}} * \frac{\boldsymbol{d^2_{C0006F}}}{\boldsymbol{d^2_{C0006E}}} = \frac{8To}{d^2{}_{C0006E}},$$

Equation 14

$$\mathrm{a_{T_{model\text{-}C0006E}}} = \frac{\frac{\mathrm{u}}{\mathrm{N}}}{\frac{8\mathrm{T}}{\mathrm{d}^2}} = \frac{\frac{\mathrm{m}}{\mathrm{rev}}}{\frac{8\mathrm{T}}{\mathrm{d}^2}} = \frac{\mathrm{md}^2{}_{\mathrm{C0006F}}}{\mathrm{rev}\,{*}8\mathrm{T}} * \frac{\mathrm{d}^2{}_{\mathrm{C0006E}}}{\mathrm{d}^2{}_{\mathrm{C0006F}}} = \frac{\mathrm{md}^2{}_{\mathrm{C0006E}}}{\mathrm{rev}\,{*}8\mathrm{T}},$$

Equation 15

$$F_{c_{model-C0006E}} = \frac{8To}{d_{C0006F}} * \frac{\boldsymbol{d_{C0006F}}}{\boldsymbol{d_{C0006E}}} = \frac{8To}{d_{C0006E}}, \textit{and}$$

Equation 16

$$\mathrm{a_{F_{model\text{-}C0006E}}} = \frac{\frac{\mathrm{u}}{\mathrm{N}}}{\frac{\mathrm{F}}{\mathrm{d}}} = \frac{\frac{\mathrm{m}}{\mathrm{rev}}}{\frac{\mathrm{F}}{\mathrm{d}}} = \frac{\mathrm{md}_{\mathrm{C0006F}}}{\mathrm{rev}\,{*}\mathrm{F}} * \frac{\mathrm{d}_{\mathrm{C0006E}}}{\mathrm{d}_{\mathrm{C0006F}}} = \frac{\mathrm{md}_{\mathrm{C0006E}}}{\mathrm{rev}\,{*}\mathrm{F}},$$

where the bolded ratio is the normalization factor that adjusts for bit-size differences across sites.

Once the appropriate normalization is applied to the model slope and threshold, $Relative\ Drillability_{F,T}$ is calculated for Holes C0006E and C0006B and displayed as the average $Relative\ Drillability_{F,T}$ (Figure 11). Despite not accounting for the difference in RCB drilling in Hole C0006F and ESCS drilling in Hole C0006E (i.e., bit efficiency), the Relative Drillability for torque at Hole C0006E overall trends about zero

residual and has similar deviations compared to the Relative Drillability at Hole C0006F below 200 mbsf. The Relative force, however, shifts positive for Hole C0006E and is most likely due to differences in coring systems (RCB vs ESCS) and the larger variation within the force model. Despite the slight variations, the comparison of the Holes C0006F and C0006E is a testament on the reproducibility of the Relative Drillability model and is further supported by the apparent correlations between deviations and identified sands/faults in the lithologic record. Further calibration between the two coring systems (bit efficiency) would most likely correct the variation of Relative force. Between 275 and 500 mbsf, there are multiple deviations to the left (easier to drill) that correlate with thrust faults and associated sands in both Holes C0006F and C0006E. It is possible the deviations are mostly due to the association of sand and the thrust faulting, as seen for the highly variable effect of sandy material at the shallow portion of the hole. Within the anomalous interval 500 to 600 mbsf of the accreted upper Shikoku Basin sediments, a shift to the left is apparent, which is possibly associated with the increased thrust faulting and ashy layering. This is also a possible indication of the over-pressured interval inferred from analysis of core samples. The lack of sharp deviations as seen in the intervals above suggests sand is not influencing the relative drillability response, and the overall interval is weakened due to localized shear/overpressure.

Hole C0006B differs somewhat from the Relative Drillability trends observed in Holes C0006E and C0006F, and is largely attributed to the difference in drilling in LWD operations. Figure 11 shows the Force Relative Drillability a full magnitude larger than that of the Torque Relative Drillability. This differs from the coring hole in which

residuals are mostly in phase and of similar amplitude to each other, and suggests the force model parameters from Hole C0006F do not fit the axial performance curve in LWD operations. To maximize resolution and obtain the best logging data, the drillers will try to control the ROP to low values and as constant as possible down the hole. When evaluating the performance curve, this has a direct impact on the axial parameters, in which the WOB is adjusted to much smaller values than that of coring operations and thus the performance curve slopes are poorly defined. The rotational parameters, however, remain consistent with those seen at Holes C0006E and C0006F. While the Relative Drillability torque fits tightly within the residual model, Hole C0006B shows no major deviations until past 600 mbsf, in which under-thrusted sand trench sediments are encountered. The lack of convergence on the residual model for the force parameters suggests the LWD holes should be evaluated and modeled separately from the coring holes.

Analysis of Outer Rise Hole C0011B

The same methodology used for Site C0006 was employed to analyze the sediments drilled at the outer rise Hole C0011B. Drilling operations at Hole C0011B began on September 5, 2009 with a 10-5/8-inch (269.88 mm) RCB BHA and tagged the water bottom at 4048.7 mbsl. RCB drilling commenced until 340 mbsf, at which coring operations began. The operation ran into a number of problems, including poor core recovery, stalls due to weather, poor borehole stability, and the discovery of the bit was completely worn after drilling to the end of the hole at a TD of 881 mbsf. A total of 329.2 m of core was recovered at an average rate of 68.1% (Saito, et al., 2010).

Figure 12 shows the result of the performance curve analysis with the resulting model fit. The best-fit coefficient values are presented in Table 3 and Table 4. Overall, the force performance curve analysis is more consistent with the functional form of systematic porosity change with depth similar to Hole C0006F while the torque performance parameters vary little with depth. The scatter of force slopes at 100 - 250 mbsf is possibly due to the increased ash layering within the shallow, unconsolidated sediments of C0011B. Within the interval 350 – 500 mbsf there is a large package of volcaniclastic sands that correlates to the main deviations reflected in the torque data. Similar to the weighing applied for the data at Hole C0006F, the sand interval between 350 – 500 mbsf is weighted lower than the other data points to account for the outliers and allow the model to be better fit to the overall character of the mud and clay-rich sediments. Overall, the performance curve behavior of Hole C0011B (Figure 12) is more variable than that of Hole C0006F, highlighting the distinction between the more unconsolidated sediments at Site C0011 versus the more tectonically deformed sediments at Site C0006 (Figure 9).

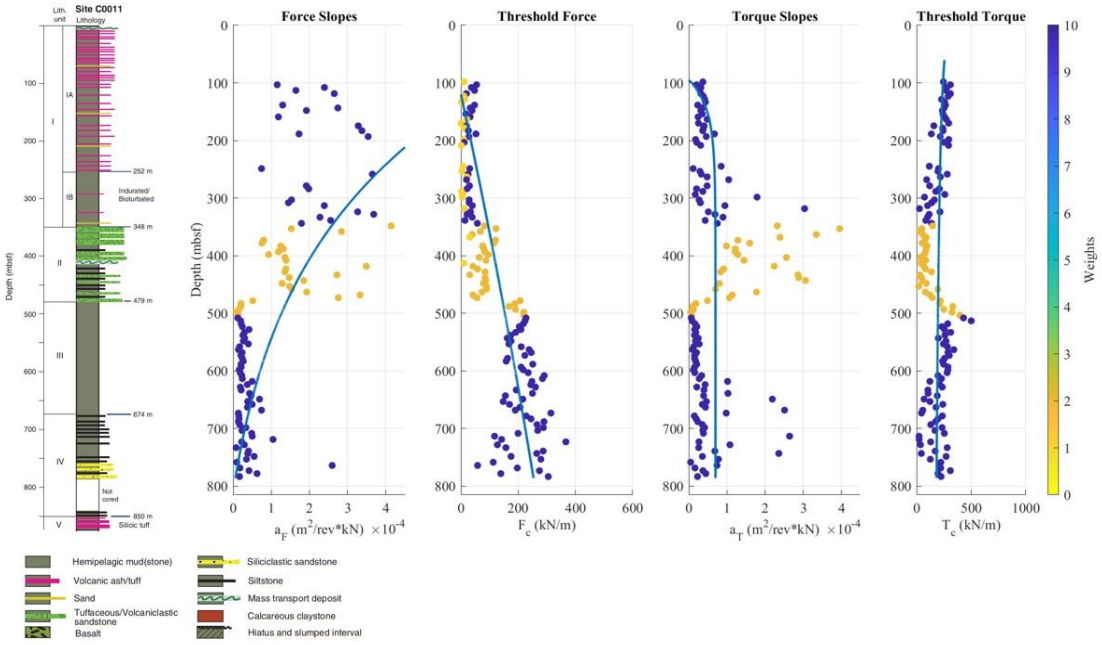

Figure 12 Performance threshold and slope data plotted versus depth with model fits, compared with lithologic column for Hole C0011B. Values are colored by weighting factors used fitting the model; sands are assigned a value of 2 out of 10. Additional weighting was given to threshold force values > 0.0005 to model the force data in the shallow region. Lithologic unit chart adapted from Saito, Underwood, Kubo, & Expedition 322 Scientists (2010).

Table 3 Hole C0011B model coefficients and associated goodness of fit (R^2) for threshold values.

	a (kN/m)	*b* (kN/m)	*c* (1/m)	R^2
$F_{c_{model}}$	-64.11	814.90	0.00058	0.80
$T_{c_{model}}$	401.00	-33.14	0.76	0.052

Table 4 Hole C0011B model coefficients and associated goodness of fit (R^2) for slope values.

	d (m^2/kN)	*e* (m^2/kN)	*f* (1/m)	*g* (.)	R^2
$a_{F_{model}}$	5.12E-03	0.0078	-0.00061	-3.25E-06	0.30
$a_{T_{model}}$	6.03E-05	-0.00035	-0.021	-3.55E-07	0.016

Comparison of Relative Drillability plots for Holes C0011B and C0006F illustrates that the Model of C0006F matches the site data more closely overall (i.e., lower average RMS) than for the model of from Hole C0011B, which demonstrates a large variability in Relative Drillability at all depths (Figure 13). This most likely reflects more uniform lithology and the tectonic loading and extensive deformation at all depths at Site C0006 that resulted in greater consolidation overall and more uniformity, similar to the model. Accordingly, the model parameters from Hole C0006F are used to evaluate the relative difference in drillability between Holes C0006F and C0011B.

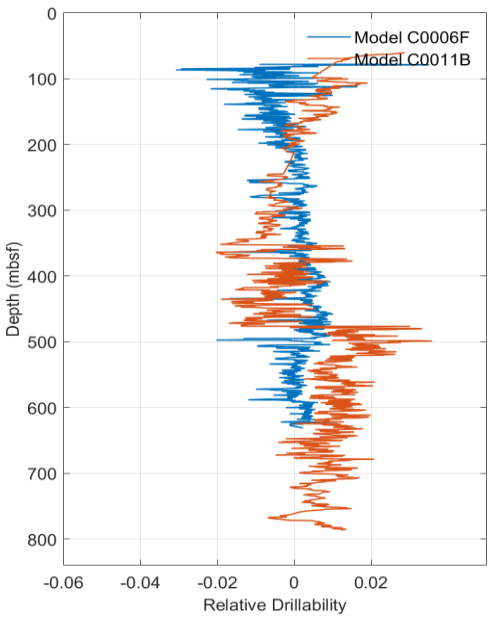

Figure 13 Comparison of Relative Drillability for Model C0006F on Hole C0006F (blue) and Model C0011B on Hole C0011B (orange).

The Relative Drillability, core porosity measurements, LWD Gamma Ray data, and lithology for both Site C0006 and Site C0011 are compared to determine if drilling data analysis can define differences in sediment response to known factors such as tectonic loading and lithologic differences (Figure 14). The accreted sediments of Unit III (450 – 603 mbsf) at Hole C0006F are correlative (time stratigraphic) to the upper Shikoku basin sediments of Unit I (100 – 250 mbsf) at Hole C0011B (Cerchiari, et al., 2018). Comparison of the Shikoku Basin sediment response at the two sites shows an overall slightly higher Relative Drillability at C0006F (~0) than at C0011B (~-.01). The subtle difference between the relative drillability was not expected due to the significantly greater magnitude tectonic loading (greater horizontal compression) at Site C0006 within the deformed accretionary toe sediments and the more extensional loading (low horizontal stress) of sediments at Site C0011within the outer rise. The porosity of the upper Shikoku basin sediments is significantly different between the two sites, as would be expected given the difference in burial depth. The measured core-porosity at Hole C0006F ranges from 40% to 60% and at Hole C0011B ranges from 60% to 70%., but both sections are consistent with the modeled depth dependence for Hole C0006F as both show very small magnitudes of relative drillability.

As discussed later, the interval 400 - 550 mbsf at Hole C0006F may have shear associated damage due to high intensity faulting that causes the Relative Drillability to be lower than normally expected relative to Hole C0011B. Despite this, the model suggests the Relative Drillability of the incoming and the accreted Shikoku basin Sediments have similar depth-corrected resistance to drilling. It is possible future

analyses that account for pump rate and for differences in bit efficiency will indicate greater differences in relative drillability for the two sites. It is reasonable to assume bit wear will have a significant impact on the performance of the bit, and the bit will be sharper when drilling the shallow sediments at Hole C0011 than the end of drilling operations at Hole C0006F.

Following these results, it is reasonable to apply the Model from C0006F to other sites of interest, including Site C0002 in the Kumano forearc basin and Sites C0004 and C0008 near the megasplay fault for further analysis. However, this also calls for quantification of model deviations and how this can directly be related to measurable rock strength (i.e., shear strength, UCS). Future work also should include experimental deformation tests to empirically calibrate the relationship of sediment strength to the model to provide a comparison of absolute strength across the various tectonic zones.

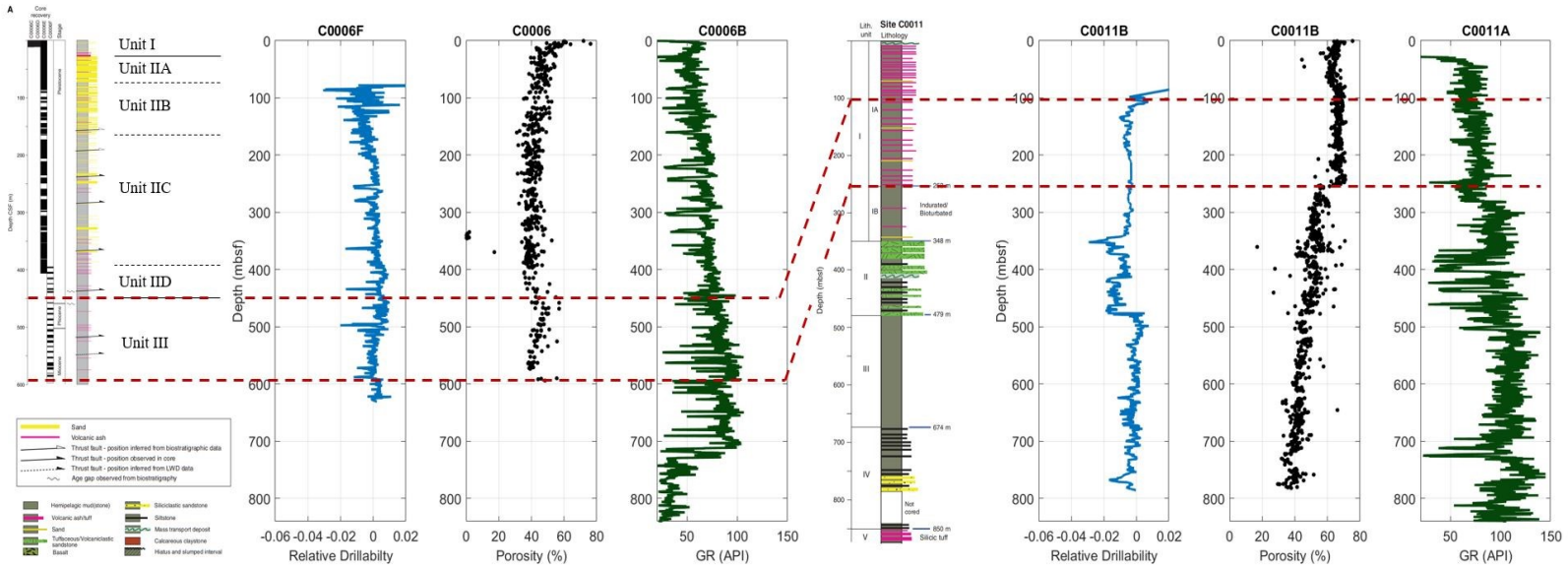

Figure 14 Comparison of Averaged Relative Drillability between Hole C0006F and Hole C0011B using model parameters from Hole C0006F. The accreted sediments in C0006F of Unit III (450 – 600 mbsf) are correlative with the upper Shikoku basin sediments at Hole C0011B (100-250 mbsf), as indicated by the red dashed lines. The Relative Drillability between the two units is similar, with an average of 0 at Hole C0006F and an average of -.01at Hole C0011B. Lithologic unit charts adapted from Kinoshita M. et al. (2009a) and Saito, Underwood, Kubo, & Expedition 322 Scientists (2010).

CHAPTER VII

FURTHER APPLICATION OF DRILLING PARAMETERS

Strength and Porosity Comparison

Following the shear strength relationship from Bingham (1964), Chester & Kitajima (written communication, 2018) also apply the intercept values (F_c, T_c) to a feasible estimation of shear strength (τ) and normal stress (σ_c). The normal stress (σ_c) is estimated as a function of the downward threshold force (F_c) and the bit diameter (d) and is as follows:

Equation 17

$$\sigma_c = k\frac{4F_c}{\pi({d_o}^2 - {d_i}^2)}$$

where k is a constant calibration, d_o is the outer diameter of the bit, and d_i is the inner diameter of the bit. Assuming that shear strength is uniform downhole, torque (T) is related to shear strength (τ) in the following equation:

Equation 18

$$T = \int_0^{2\pi}\int_{r_i}^{r_o} \tau * r\, dr\, d\theta = 2\pi \int_{r_i}^{r_o} r^2\, dr = \frac{2\pi\tau}{3}({r_o}^3 - {r_i}^3)$$

where r_o and r_i are the outer bit radius and inner bit radius, respectfully. Equation 18 is rearranged to solve for the shear strength (τ) and equate torque (T) to threshold torque (T_c) as follows:

Equation 19

$$\tau = k\frac{3T_c}{2\pi({r_o}^3 - {r_i}^3)} = k\frac{24T_c}{2\pi({d_o}^3 - {d_i}^3)}$$

where constant k is a constant calibration. The resulting τ , therefore, represents a shear value for each depth interval and is compared to vane shear and penetration data (Figure 15) (Kinoshita M. et al., 2009a).

Independent determinations of strength for the sediments in the boreholes is provided by shear/penetration measurements (Kinoshita M., 2009a). Using these data, the constant k is assigned a value of 0.2 to fit the shear/penetration measurement data. The constant k is the estimate of the total energy that is actually cutting the rock at the bit and is less than one due to energy losses elsewhere. Further experimental calibration is required to accurately relate the threshold values from drilling parameter data with measurable rock strength values. Despite this, changes in the vane shear strength and penetration measurements and the shear/normal stress predictions made from the threshold values of drilling parameter data are similar. Overall, the strength determined from drilling data are approximately proportional to depth as would be expected for marine sediments. This supports the original hypotheses by Teale (1965) and Bingham (1964) suggesting the onset of bit penetration (i.e., threshold) can be correlated with a measurable quantity of rock strength.

As observed in Chapter V, the depth interval 400 – 550 mbsf has anomalously higher strength values than the overlying and underlying sediments (Figure 15). Within this interval we would expect the strength to decrease with the anomalously high porosities reported from the cores. Evaluation of the raw drilling data in Figure 4 shows the pump rate (Active SPM) was lowered within this interval as the WOB was increased. This is the most likely cause of the unexpected increase in threshold force, and could be

the response to either the lithology or presence of an over pressured zone, or a combination thereof. The core analysis suggests the highest values of porosity within 450 – 490 mbsf are a result of fault damage or unconsolidated sediments with elevated fluid pressures attributing to localized shear deformation. The increased presence of clay within this interval also suggests more impermeable pathways, allowing elevated pore pressures to develop and therefore increased porosity. From 490 to 570 mbsf, the porosity values begin to decrease with depth, although still lower in comparison to the trend from shallower porosity values. This effect is explained by either fault damage from the intervals 434 to 490 mbsf and 533 – 560 mbsf or evidence of over pressured fluids (Kinoshita M. , et al., 2009a). The possible effect of the pump rate on the drilling parameter response suggests the need for some pump rate normalization of the data. This suggestion is not explored within this work, but proposed for future consideration.

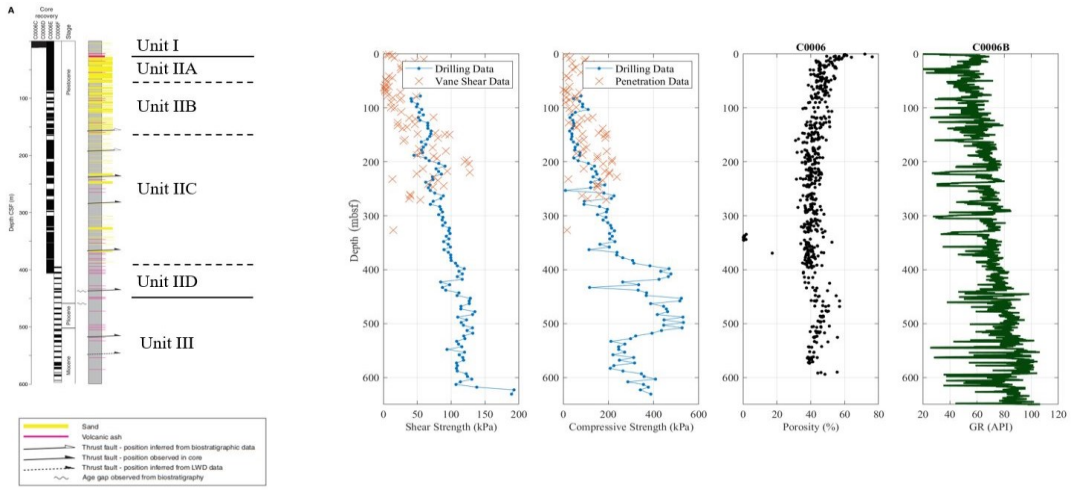

Figure 15 Shear and compressive strength profiles determined from the drilling data for Hole C0006F compared to porosity, natural gamma ray and lithology with depth. Vane shear and penetration data (orange) is derived from Site C0006 core measurements and used to calibrate the absolute strength of drilling estimates. Lithologic unit chart adapted from Kinoshita M. et al., 2009a.

CHAPTER VIII

DISCUSSION

The results of this project demonstrate the methodology introduced to evaluate drilling parameter data derived from IODP scientific drilling of marine sediments in performance space (i.e., penetration rate versus rotational and axial energy) is a viable approach to characterize relative changing in sediment strength with depth due to burial to the first order and to lithologic variation and tectonic deformation to the second order (Figure 7). Following the observation that the logarithm of drilling-performance threshold values increase linearly with decreasing sediment porosity (determined from core-sample analysis; Figure 8), and the geophysical evidence that the porosity - depth relationship for marine sediments approximately follows an exponential form, we propose equations (Equation 10 and Equation 11) to model the changes in drilling-performance threshold and slope values as a function of depth. Applying the model equations to data from drilling the tectonically deformed sediments at Site C0006 indicates the equations adequately describe the overall depth-dependent trends (fairly high R-squared values of 0.6-0.9), supporting the use of the proposed functional forms for marine sediments.

Given the success of the model to characterize the depth-dependence of sediment response for a site, relationships are proposed to quantify the Relative Drillability (Equation 12) , i.e., deviations from the reference model, in order to document local variations in sediment response arising from changes in lithology (interbedded sands in mud-dominated units) and deformation by fracturing and faulting (Figure 11).

Application of Relative Drillability using Hole C0006F modeling parameters successfully highlights local changes due to lithology and concentrated deformation, as well as a subtle change in sediment response between the tectonically deformed sediments at Hole C0006F and the slightly easier to drill, normally consolidated sediments at Hole C0011B (Figure 14).

On the basis of the ability to relate drilling response to geologic and geophysical parameters, and previous work relating drilling response parameters with rock strength, equations (Equation 17 and Equation 19) are presented to determine sediment strength as a function of depth from drilling-performance data. The equations are used to relate the axial and rotational threshold values to normal and shear strength, but they include a unknown factor that reflects potential differences between drilling parameters measured at the bit and those measured at the surface as in IODP drilling. As such, the factor must be determined to make robust determinations of absolute strength from drilling data; however, relative strength determinations should be sound employing the methodologies herein. Unfortunately, there is relatively little independent information on strength of sediments drilled along the NanTroSEIZE transect with which to calibrate the unknown factor in the equations to determine strength. Here, the strength relations are approximately calibrated to match the approximate sediment strength from shipboard vane shear and penetration measurements of the core samples at site C0006 (Figure 15).

The methodology and case study results of this project are a significant advance in relating drilling parameter relationships to marine sediment strength in order to quantify deviations in sediment strength due to burial, tectonic stresses, lithology, and

presence of faulting. In general, the sediments within the accretionary prism (e.g., Site C0006) are overall harder to drill, and therefore inferred as stronger, than those on the incoming plate at the outer rise (e.g., Site C0011). We would expect, then, that application of the performance curve analysis including depth-dependent modeling and relative drillability methods at other NanTroSEIZE sites would provide further insight into the sediment behavior of the prism between the Kumano forearc basin sediments, the older accretionary prism, and underthrust/ overthrust sediments near the megasplay fault zone.

Overall, the results here build on the initial advances for rock presented by Bingham (1964), Teale (1965), and Karasawa et al. (2002) to apply analysis and modeling for marine sediments. During the period of this project, Hamada et al. published an analysis of drilling data at NanTroSEIZE Site C0002, where the Kumano forearc basin and the underlying accretionary prism were drilled to significant depth (Hamada et al.,2018a), and of IODP Site C0023 where drilling crossed the Nankai plate-boundary decollement (Hamada et al.,2018b). Hamada et al. (2018a) introduce an approach to analyze the performance space for axial and rotational components simultaneously, as well as a technique to estimate frictional losses of energy associated with the drill stem. A method to determine the strength of sediments referred to as the equivalent strength (EST) is presented. Similar to the calculation of strength from drilling data herein, their relationship also requires calibration from independent measures of sediment strength. Interestingly, estiments of sediment strength by Hamada et al. (2018a, b) are significantly larger than other estimates, including the estimates

herein. Overall, the findings of Hamada et al. (2018a, b) are consistent with the findings of this project in that the drilling parameters do reflect changes of sediment strength locally and with depth.

From the analysis herein, it is evident that further normalization of controlling parameters such as pump rate and bit efficiency is required to constrain the models and determine sediment strength. In addition to normalization of the data, experimental work is needed to quantify the empircal relationship between our presented models and absolute strength of sediments. This study was limited by the quality of data, including lack of downhole measurements of torque and WOB to account for drill string friction associated energy loss, but also only having a sampling rate of 0.1 Hz or lower. A sampling rate of 1 Hz would be preferred in order to capture subtle strength changes and to better correlate WOB and Torque measurements to ROP. Lastly, the apparent success in using drilling data to produce continuous determination of marine sediment strength with depth suggests that collaboration of scientists and drilling engineers to optimize drilling operations for collecting meaningful drilling parameter data could improve data quality and advance analysis methodology for robust determinations of the mechanical properties of marine sediments.

CHAPTER IX

CONCLUSION

This project presents a methodology to relate drilling performance curve parameters to marine sediment strength within the Nankai Trough. Analysis and modeling of IODP Drilling Hole C0006F indicates a systematic change in performance curve parameters (threshold and slope) with depth that follows the expected change in strength associated with increasing depth from burial loading and dewatering of marine sediments. On the basis of the depth-dependent models, Relative Drillability calculations are introduced to capture local changes of strength due to lithology, faulting, and varying tectonic stressing. Overall, variations in Relative Drillability are observed at depth intervals of thrust faulting and lithologic units other than the dominant lithology of muds and clayey sediments (e.g., sands), supporting the hypothesis that weaker and stronger depth intervals have a local effect on the drilling response.

The methodology herein is one of the first to apply drilling parameter analysis to marine sediments, and as such there are additional considerations for future work. These considerations include quantifying the absolute strength of sediments determined from the depth-dependent model and the deviations identified via Relative Drillability, which requires carefully designed experimental studies of sediment strength for model calibration. In addition, consideration of normalization techniques to adjust for drilling practices (e.g., bit efficiency, pump rates and mud weights). Once the models are calibrated, it would be prudent to then apply the methodology to more sites along the

NanTroSEIZE transect to fully evaluate the sediment strength changes across the different tectonic zones and apply the derived continuous strength-depth profiles in other appropriate applications (e.g., in situ stress analyses, borehole breakout analysis).

REFERENCES

Anderson, E. M. (1905). The dynamics of faulting. *Transactions of the Edinburgh Geological Society, 8*, 387-402.

Athy, L. F. (1930). Density, Porosity, and Compaction of Sedimentary Rocks. *Bulletin of the American Association of Petroleum Geologists, 14*(1).

Bahr, D. B., Hutton, E. W., Syvitski, J. P., & Pratson, L. F. (2001). Exponential approximations to compacted sediment porosity profiles. *Computers and Geosciences, 27*, 691-700.

Baldauf, J., Becker, K., Davis, E., Davies, T., Fox, P. J., Graber, K. K., . . . Schroeder, D. (2004). Overview of Ocean Drilling Program Engineering Tools and Hardware: Core Bits. (K. K. Graber, E. Pollard, B. Jonasson, & E. Schulte, Eds.) *Ocean Drilling Program*.

Bangs, N., Moore, G., Gulick, S., Pangborn, E., Tobin, H., Kuramoto, S., & Taira, A. (2009). Broad, weak regions of the Nankai Megathrust and Implications for shallow coseismic slip. *Earth and Planetary Science Letters*, 44-49.

Bingham, M. G. (1964). How Rock Properties Are Related to Drilling. *Oil and Gas Journal, 62*(50), 94-99.

CDEX Technical Report Drilling Completion Report NanTroSEIZE Stage 2 IODP Expedition 319 and 322. (2010). The Center for Deep Earth Exploration.

Cerchiari, A., Fukuchi, R., Gao, B., Hsiung, K.-H., Jaeger, D., Kaneki, S., . . . Yabe, S. (2018). IODP workshop: Core-Log Seismic Investigation at Sea - Integrating

legacy data to address outstanding reserach questions in the Nankai Trough Seismogenic Zone Experiment. *Scientific Drilling, 24*, 93-107.

Chang, C., McNeill, L. C., Moore, J. C., Lin, W., Conin, M., & Yamada, Y. (2010). In situ stress state in the Nankai accretionary wedge estimated from borehole wall failures. *Geochemisty. Geophysics . Geosystems., 11*, 1-17.

Chang, C., Zoback, M., & Khaksar, A. (2006). Empirical relations between rock strength and physical properties in sedimentary rocks. *Journal of Petroleum Science and Engineering, 51*, 223-237.

DeMets, C., Gordon, R. G., & Argus, D. F. (2010). Geologically current plate motions. *Geophysical Journal International*.

Hamada, Y., Hirose, T., Ijiri, A., Yamada, Y., Sanada, Y., Saito, S., . . . Heuer, V. B. (2018b). In-situ mechancial weakness of subducting sediments beneath a plate boundary decollement in the Nankai Trough. *Progress in Earth and Planetary Science, 5*(70).

Hamada, Y., Kitamura, M., Yamada, Y., Sanada, Y., Sugihara, T., Saito, S., . . . Hirose, T. (2018a). Continuous depth profile of the rock strength in the Nankai accretionary prism based on drilling performance parameters. *Scientific Reports*, 1-9.

Henry, P., Kanamatsu, T., Moe, K., & Expedition 333 Scientists. (2012). Expedition 333 summary. *Proceedings of the Integrated Ocean Drilling Program, 333*.

Holtz, R. D., Kovacs, W. D., & Sheahan, T. C. (2011). *An Introduction to Geotechnical Engineering (Second Edition).* Upper Saddle River: Pearson Education, Inc.

Huffman, K., Saffer, D., & Dugan, B. (2016). In situ stress magnitude and rock strength in the Nankai accretionary complex: a novel approach using paired constraints from downhole data in two wells. *Earth, Planets, and Space, 68*(123), 1-9.

Kanamori, H. (1972). Tectonic Implications of the 1944 Tonankai and the 1946 Nankaido earthquakes. *Physics of the Earth and Planetary Interiors, 5*, 129-139.

Karasawa, H., Ohno, T., Kosugi, M., & Rowley, J. (2002). Methods to Estimate the Rock Strength and Tooth Wear While Drilling With Roller-Bits --Part 1: Milled-Tooth Bits. *Journal of Energy Resources Technology, 124*, 125-132.

Karig, D., & Ask, M. (2003). Geological perspectives on consolidation of clay-rich marine sediments. *Journal of Geophysical Research: Solid Earth, 108*(B4).

Karig, D., & Morgan, J. (1994). Tectonic deformation: stress paths and strain histories. In M. A., *The Geological Deformation of Sediments* (pp. 167-204). Springer, Dordrecht.

Karner, S. L., Chester, J. S., Chester, F. M., Kronenberg, A. K., & Hajash Jr., A. (2005). Laboratory deformation of granular quartz sand: Implications for the burial of clastic rocks. *AAPG Bulletin, 89*(5), 603-625.

Kerkar, P., Hareland, G., Fonseca, E., & Hackbarth, C. (2014). Estimation of Rock Compressive Strength using Downhole Weight-on-Bit and Drilling Models. *International Petroleum Technology Conference*, (pp. 1-12). Doha, Qatar.

Kinoshita, M., Tobin, H., Ashi, J., Kimura, G., Lallemant, S., Screaton, E., . . . Expedition 314/315/316 Scientists. (2009a). Expedition 316 Site C0006. *Proceedings of the Integrated Ocean Drilling Program, 314/315/316*, 1-124.

Kinoshita, M., Tobin, H., Ashi, J., Kimura, G., Lallemant, S., Screaton, E., . . . Expedition 314/315/316 Scientists. (2009b). NanTroSEIZE Stage 1 expeditions: introduction and synthesis of key results. *Proceedings of the Integrated Ocean Drilling Program, 314/315/316*, 1-20.

Kinoshita, M., Tobin, H., Ashi, J., Kimura, G., Lallemant, S., Screaton, E., . . . Expedition 314/315/316 Scientists. (2009c). Expedition 314 Site C0006. *Proceedings of the Integrated Ocean Drilling Program, 314/315/316*.

Kitajima, H., Chester, F. M., & Biscontin, G. (2012). Mechancial and hydraulic properties of Nankai accretionary prism sediments: Effect of stress path. *Geochemistry. Geophysics. Geosystems, 13*(1), 1-24.

Kobayashi, S., Muta, K., Sawada, I., Abe, T., Saruhashi, T., Higuchi, K., . . . Kawano, Y. (2008). *CDEX Technical Report Drilling Completion Report NanTroSEIZE Stage 1 IODP Expedition 314, 315, and 316* (Vol. 4). Yokohama, Japan: Center for Deep Earth Exploration, Japan Agency for Marine-Earth Science and Technology.

Lin, W., Byrne, T., Kinoshita, M., McNeill, L., Chang, C., Lewis, J., . . . Kanamatsu, T. (2016). Distribution of stress state in the Nankai subduction zone, southwest Japan and comparison with Japan Trench. *Tectonophysics, 692*, 120-130.

Mitchell, R. F., & Miska, S. Z. (2011). *Fundamentals of Drilling Engineering* (Vol. 12). Richardson, TX: Society of Petroleum Engineers.

Moore, G. F., Bangs, N. L., Taira, A., Kuramoto, S., Pangborn, E., & Tobin, H. J. (2007). Three-Dimensional Splay Fault Geometry and Implications for Tsunami Generation. *Science, 318*(5853), 1128-1131.

Moore, G., Park, J., Bangs, N., Gulich, S., Tobin, H., Nakamura, Y., . . . Taira, A. (2009). Structural and seismic stratigraphic framework of teh NanTroSEIZE Stage 1 transect. *Proceedings of the Integrated Ocean Drilling Program, Volume 314/315/316*, 1-46.

Moore, G., Shipley, T. S., Karig, D., Taira, A., Kuramoto, S., & Suyehiro, K. (1990). Structure of the Nankai Trough accretionary zone from mulitchannel seismic reflection data. *Journal of Geophysical Research: Solid Earth, 95*(B6), 8753-8765.

Moore, J. C., & Saffer, D. (2001). Updip limit of the seismogenic zone beneath the accretionary prism of southwest Japa: An effect of diagenetic to low-grade metamorphic processes and increaseing effective stress. *Geology, 29*, 183-186.

Ohno, T., Karasawa, H., Kosugi, M., & Rowley, J. (2004). Proposal Practical Methods to Estimate Rock Strength and Tooth Wear While Drilling with Roller-Cone Bits. *Journal of Energy Resources Technology, 126*, 302-310.

Park, J.-O., Tsuru, T., No, T., Takizawa, K., Sato, S., & Kaneda, Y. (2008). A high-resolution 3D seismic reflection survey and prestack depth imaging in the Nankai Trough off southeast Kii Peninsula. *BUTSURI-TANSA(Geophysical Exploration), 61*(3), 231-241.

Saffer, D., Guo, J., Underwood, M., Likos, W., Skarbek, R., Song, I., . . . Expedition 314/315/316 Scientists. (2011). Data report: consolidation, permeability, and fabric of sediments from the Nankai continental slope, IODP Sites C0001, C0008, and C0004. *Proceedings of the Integrated Ocean Drilling Program, Volume 314/315/316*, 1-61.

Saito, S., Underwood, M., Kubo, Y., & Expedition 322 Scientists. (2010). Site C0011. *Proc. IODP, 322*.

Shi, X., Meng, Y., Li, G., Tao, Z., & Wei, S. (2015). Confined compressive strength model of rock for drilling optimization. *Petroleum, 1*, 40-45.

Song, I., Saffer, D. M., & Flemings, P. B. (2011). Mechanical characterization of slope sediments: Constraints on in situ stress and pore pressure near the tip of the megasplay fault in the Nankai accretionary complex. *Geochemistry. Geophysics. Geosystems., 12*(5), 1-20.

Teale, R. (1965). The concept of specific energy in rock drilling. *Int. J. Rock Mech. Mining Sci., 2*, 57-73.

Terzaghi, K., Peck, R., & Mesri, G. (1996). *Soil mechanics in engineering practice* (3rd ed.). New York: John Wiley and Sons.

Tobin, H., & Kinoshita, M. (2007). The IODP Nankai Trough Seismoenic Zone Experiment. *Scientific Drilling Special*(1), 39-41.

Tobin, H., Kinoshita, M., Ashi, J., Lallemant, S., Kimura, G., Screaton, E., . . . Expedition 314/315/316 Scientists . (2009). NanTroSEIZE Stage 1 expeditions:

introduction and synthesis of key results. *Proceedings of the Integrated Ocean Drilling Program*.

Wang, K., & Hu, Y. (2006). Accretionary prisms in subduction earthquake cycles: The theory of dynamic Coulomb wedge. *Journal of Geophysical Research, 111*(B06410), 1-16.

Wang, K., & Yan, H. (2006). Accretionary prisms in subduction earthquake cycles: The theory of dynamic Coulomb wedge. *Journal of Geophysical Research*.

Warren, T. M. (1984). Factors Affecting Torque for a Roller Cone Bit. *Journal of Petroleum Technologies, 36*, 1500-1508.

Wong, T. f., David, C., & Zhu, W. (1997). The transition from brittle faulting to cataclastic flow in porous sandstones: Mechancial deformation. *Journal of Geophysical Research, 102*(B2), 3009-3025.

Wood, D. (1990). *Soil Behavior and Critical State Soil Mechanics.* Cambridge: Cambridge University Press.

APPENDIX

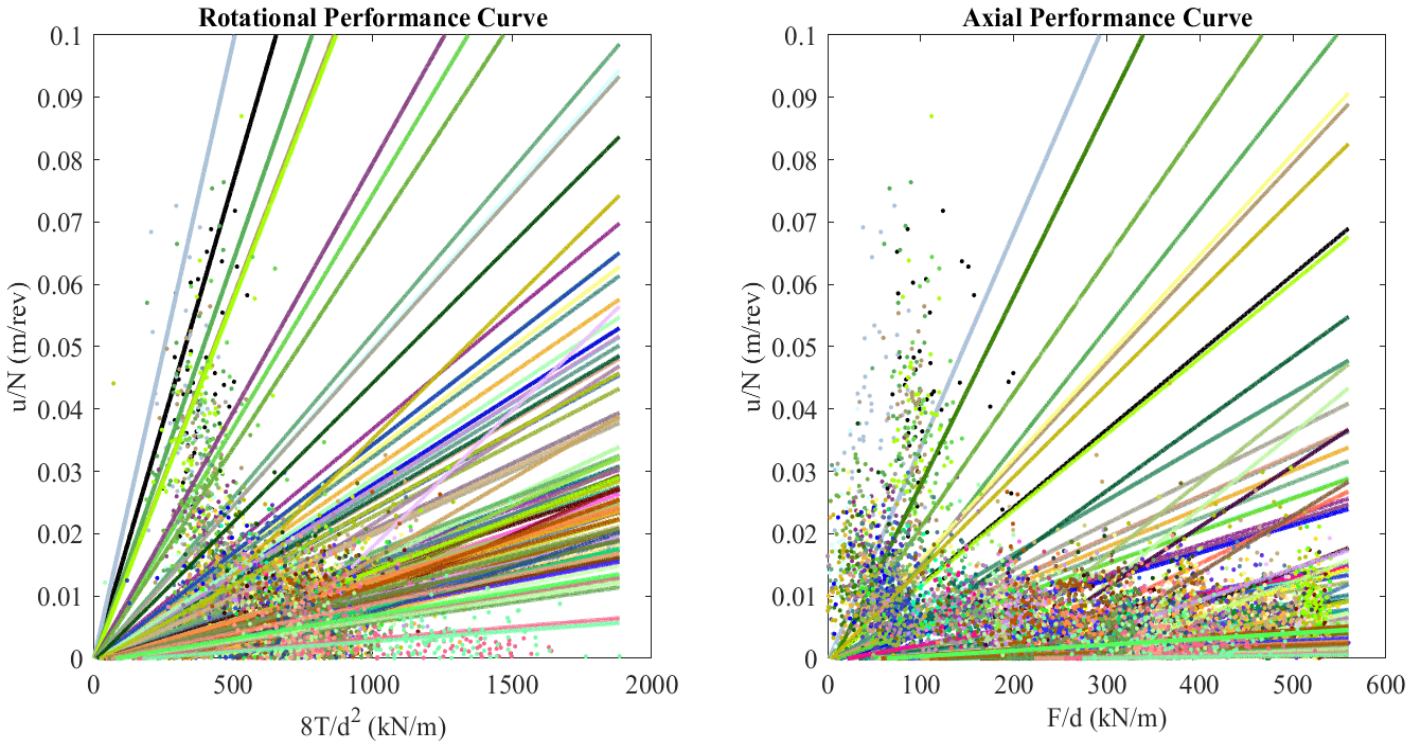

Figure 16 Performance curve analysis of Hole C0006F at 5 m intervals.

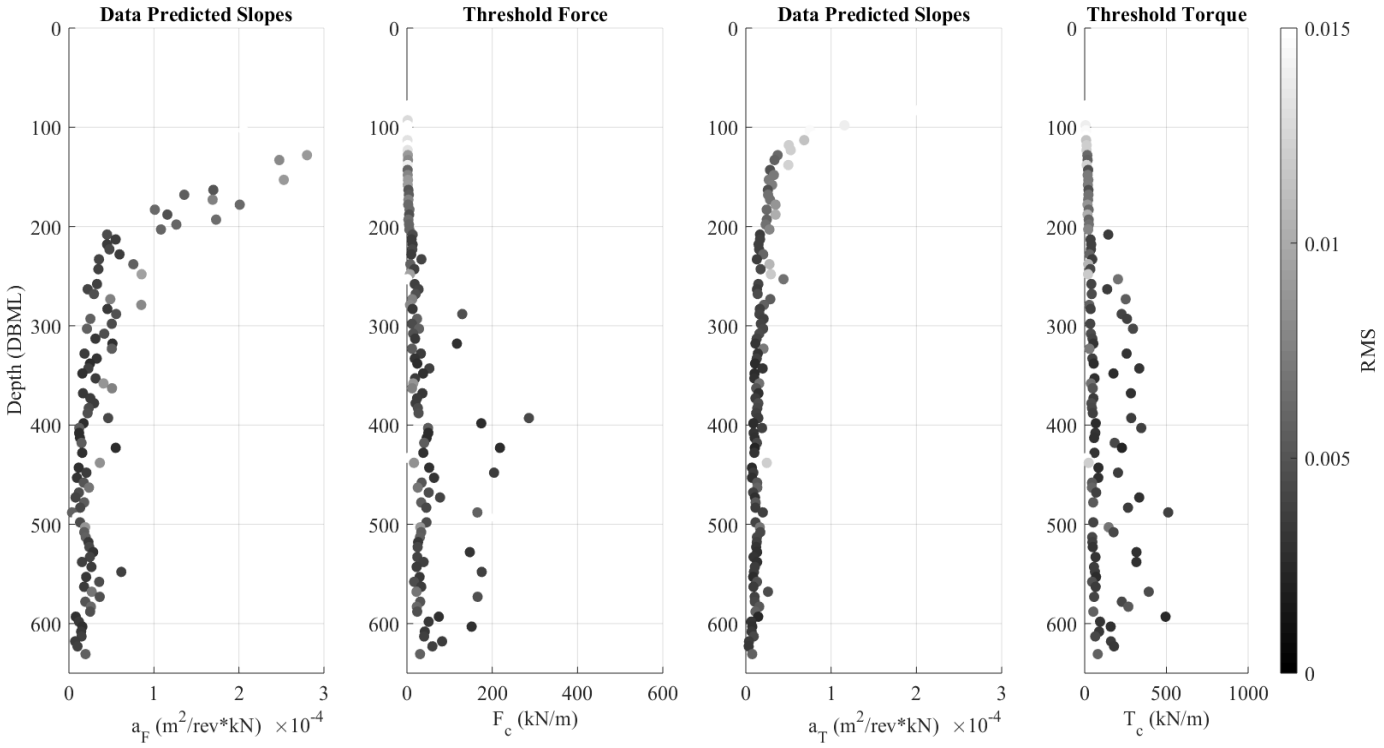

Figure 17 Performance curve parameter analysis at Hole C0006F. Threshold force and torque are picked at $\frac{\boldsymbol{u}}{\boldsymbol{N}} = 0$, as opposed to the offset $\frac{\boldsymbol{u}}{\boldsymbol{N}}_{10\%\ trq\ bit}$ and $\frac{\boldsymbol{F}}{\boldsymbol{d}}, \frac{\boldsymbol{8T}}{\boldsymbol{d^2}}_{10\%\ trq\ bit}$. MBSF is the equivalent of mbsf.

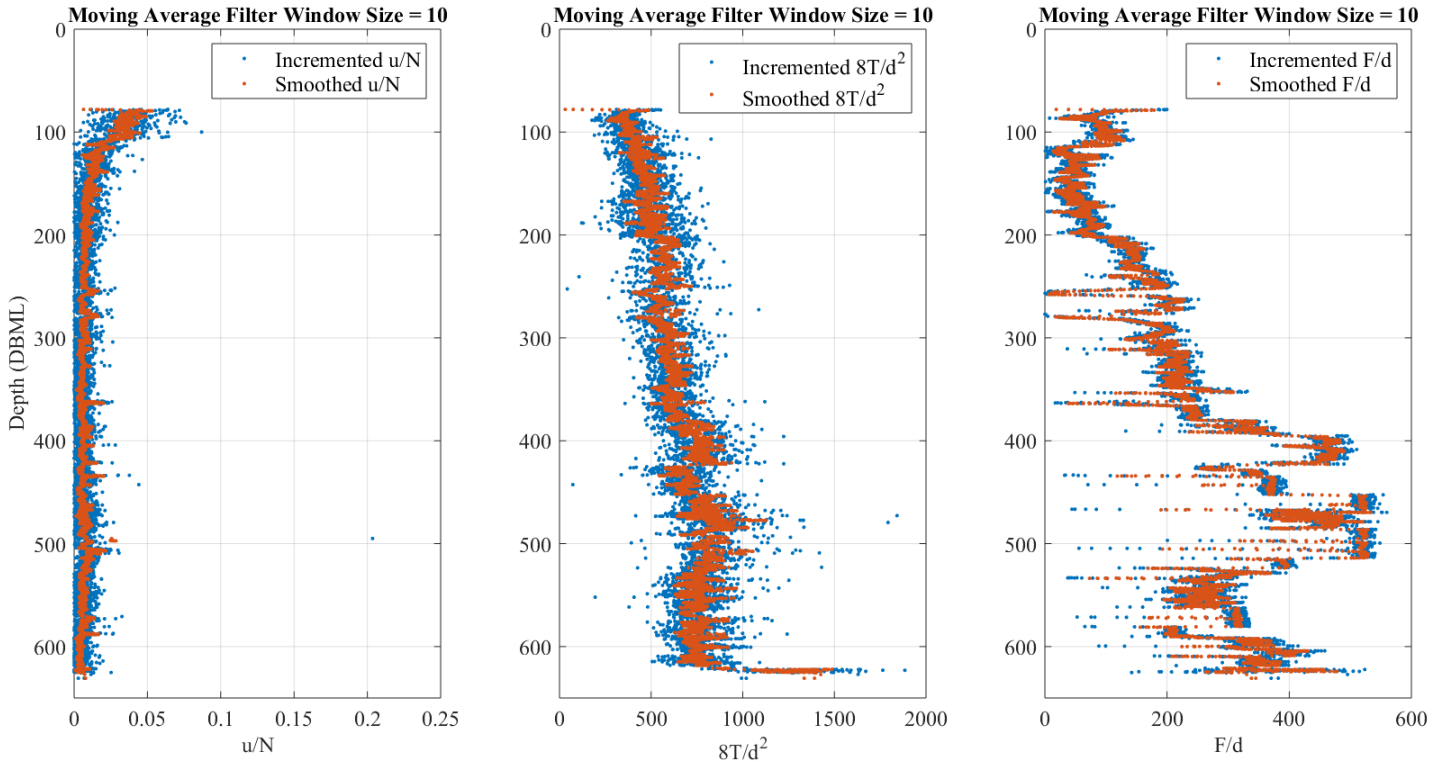

Figure 18 Smoothed parameter data ($\frac{\boldsymbol{u}}{\boldsymbol{N}_{obs}}$ and $\frac{\boldsymbol{F}}{\boldsymbol{d}}$, $\frac{\boldsymbol{8T}}{\boldsymbol{d^2}_{obs}}$) for Relative Drillability. MBSF is the equivalent of mbsf.

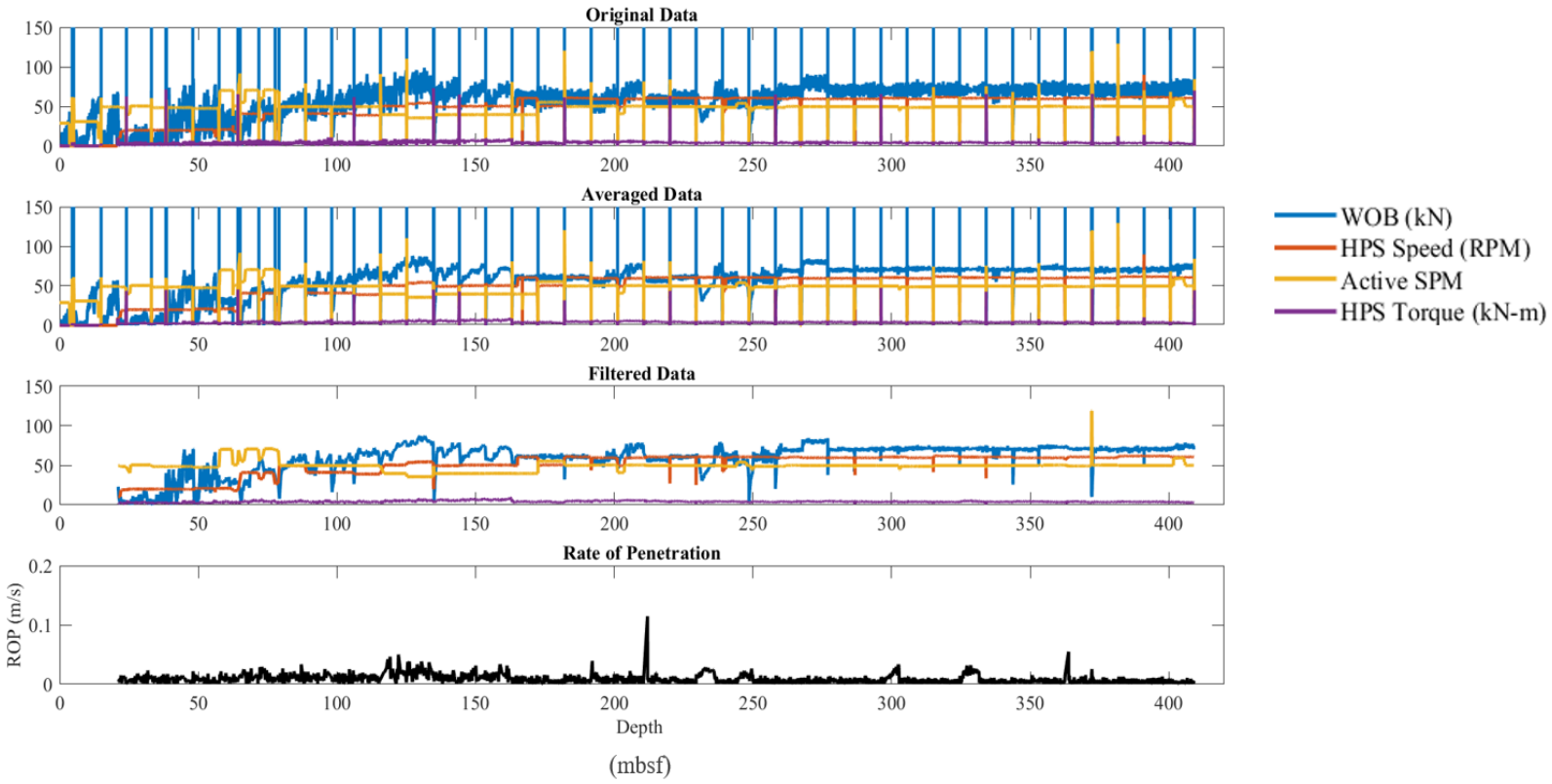

Figure 19 Original and processed data for Hole C0006E.

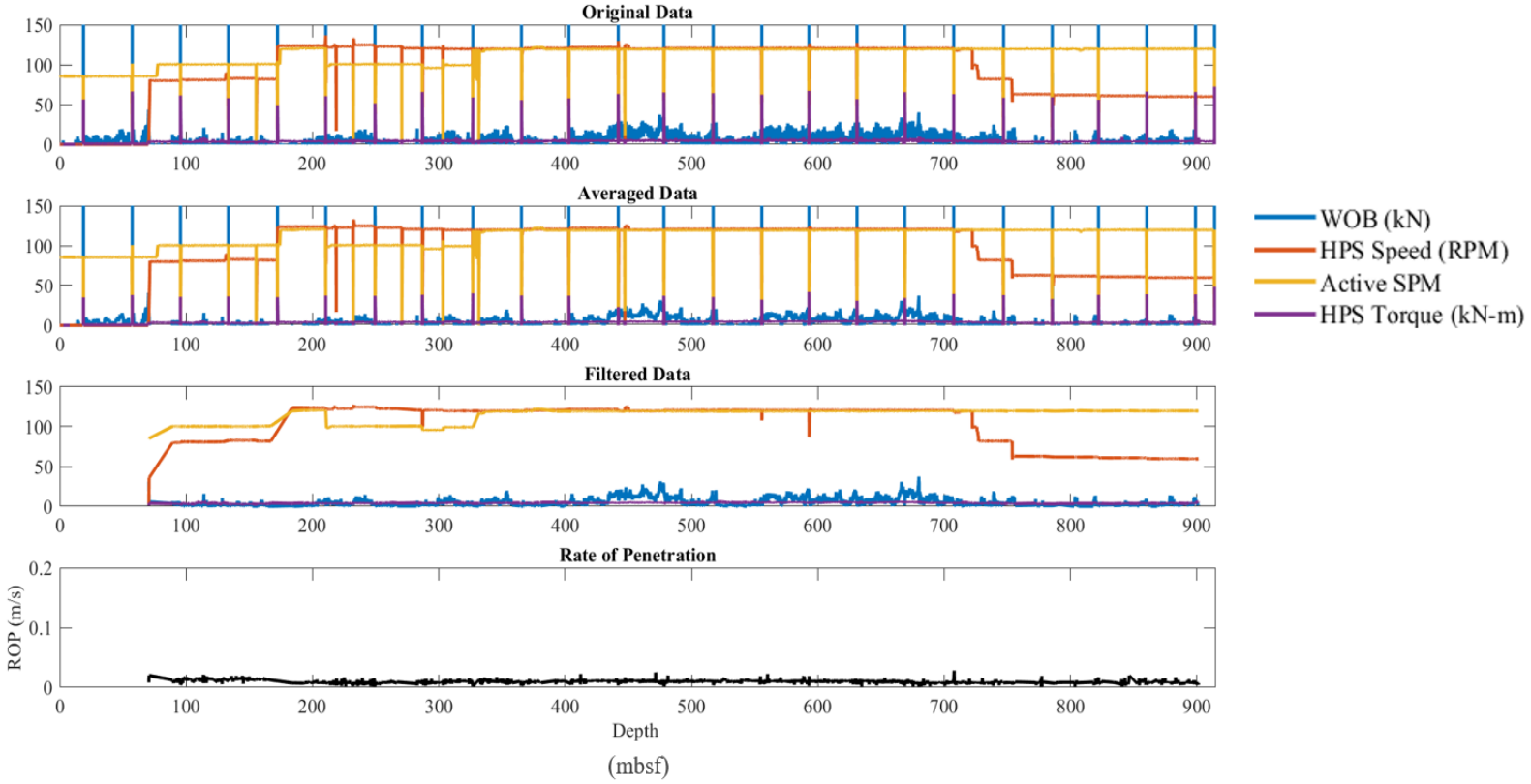

Figure 20 Original and processed data for Hole C0006B.

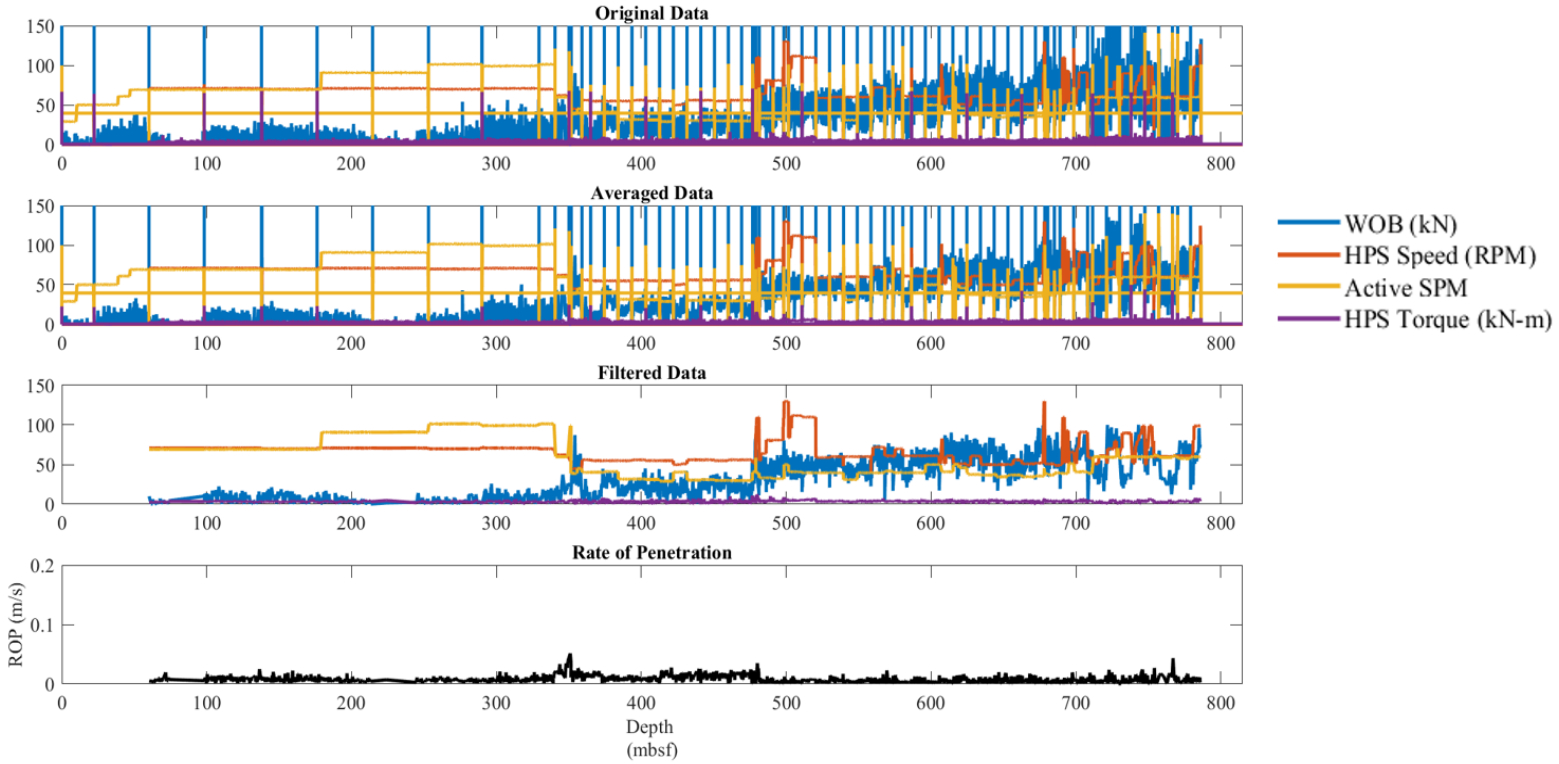

Figure 21 Original and processed data for Hole C0011B.

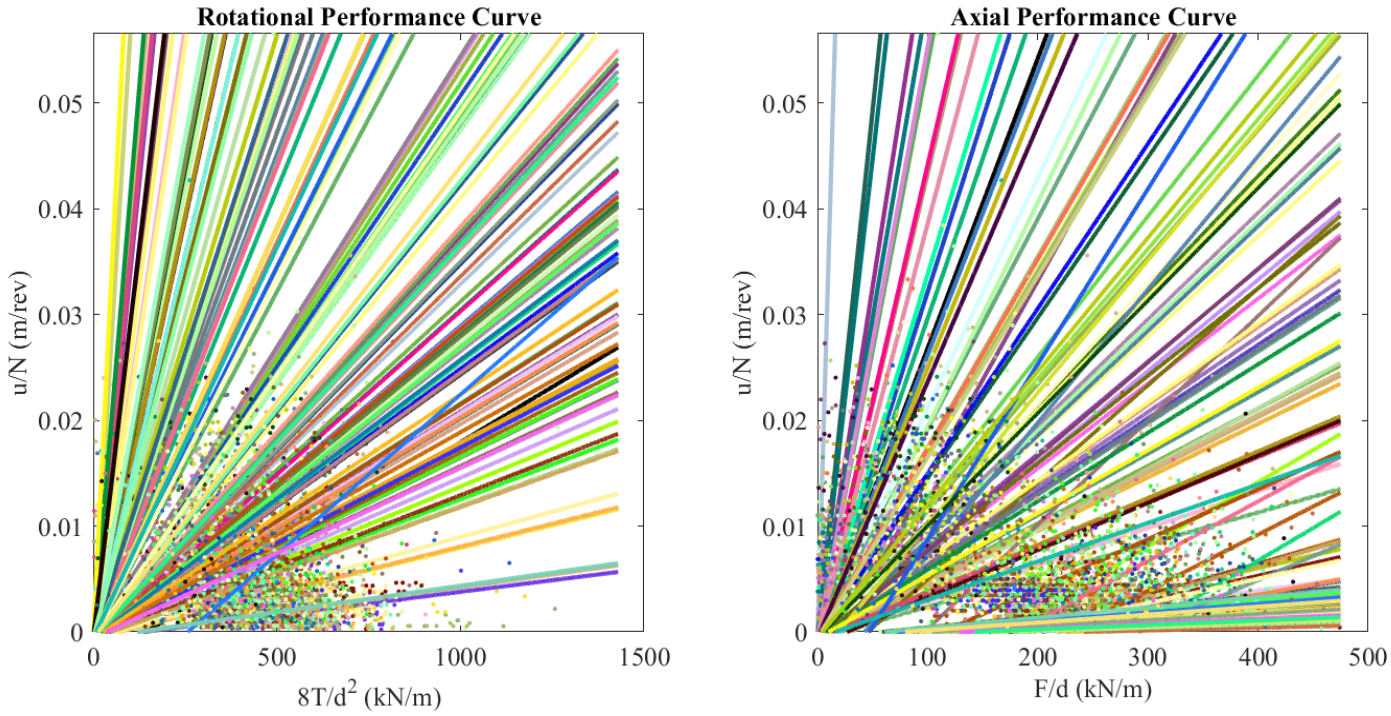

Figure 22 Performance curve analysis of Hole C0011B at 5 m intervals.

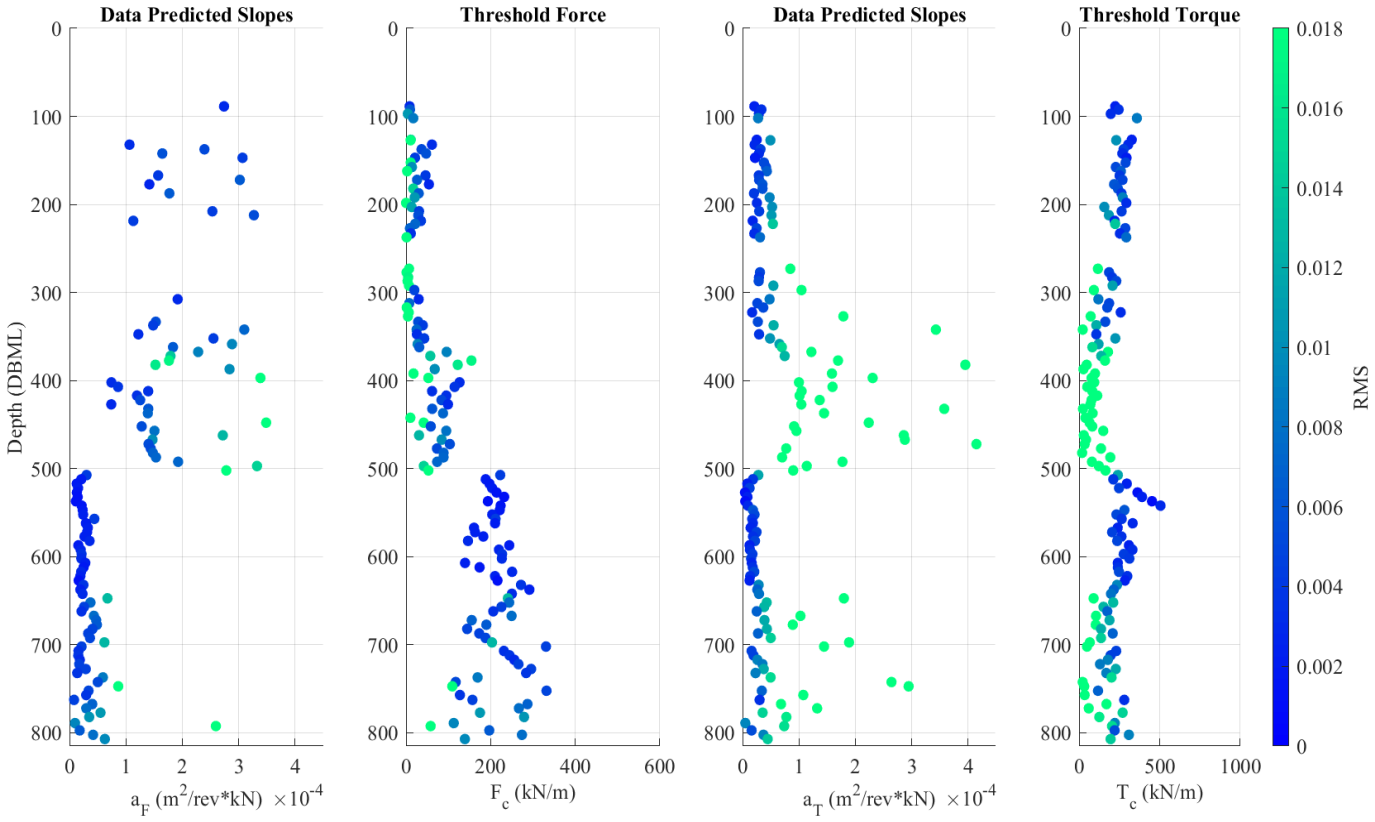

Figure 23 Performance curve analysis of Hole C0011B. Data colored by RMS value. MBSF is the equivalent of mbsf.